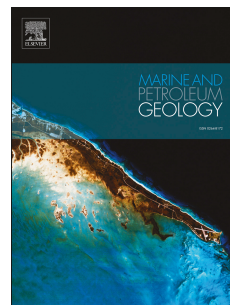


Journal Pre-proof

Late Cretaceous coeval multi-directional extension in southeastern Zealandia:
Implications for eastern Gondwana breakup

A. Barrier, A. Nicol, G.H. Browne, K.N. Bassett



PII: S0264-8172(20)30166-5

DOI: <https://doi.org/10.1016/j.marpetgeo.2020.104383>

Reference: JMPG 104383

To appear in: *Marine and Petroleum Geology*

Received Date: 2 October 2019

Revised Date: 31 March 2020

Accepted Date: 1 April 2020

Please cite this article as: Barrier, A., Nicol, A., Browne, G.H., Bassett, K.N., Late Cretaceous coeval multi-directional extension in southeastern Zealandia: Implications for eastern Gondwana breakup, *Marine and Petroleum Geology* (2020), doi: <https://doi.org/10.1016/j.marpetgeo.2020.104383>.

This is a PDF file of an article that has undergone enhancements after acceptance, such as the addition of a cover page and metadata, and formatting for readability, but it is not yet the definitive version of record. This version will undergo additional copyediting, typesetting and review before it is published in its final form, but we are providing this version to give early visibility of the article. Please note that, during the production process, errors may be discovered which could affect the content, and all legal disclaimers that apply to the journal pertain.

© 2020 Published by Elsevier Ltd.

1 **LATE CRETACEOUS COEVAL MULTI-DIRECTIONAL**

2 **EXTENSION IN SOUTHEASTERN ZEALANDIA:**

3 **IMPLICATIONS FOR EASTERN GONDWANA BREAKUP**

4

5 **A. Barrier¹, A. Nicol¹, G.H. Browne² and K.N. Bassett¹**

6 ¹*University of Canterbury, School of Earth and Environment, Christchurch, New Zealand.*

7 ²*GNS Science, PO Box 30368, Lower Hutt, New Zealand.*

8 Corresponding author:

9 Andrea Barrier –barrierandrea@gmail.com

10

11 **Abstract**

12 Gondwana continental crust in southeastern Zealandia was deformed by Cretaceous rift faults with
13 multiple orientations. Our interpretation of 2D and 3D seismic reflection lines, tied to wells in the
14 Canterbury Basin of southeastern Zealandia, shows three coeval sets of faults with trends of NE-
15 SW, E-W and NW-SE. Geometric and displacement analyses of segmented faults from each set
16 suggests that they mainly accommodated normal dip-slip, producing multi-directional stretching in
17 Zealandia. Growth strata indicate that the three fault sets were active synchronously over ~20 Myr
18 from ~105 to ~85 Ma. The fault sets are present throughout Zealandia and roughly parallel to
19 spreading centres produced during Gondwana breakup, primarily defining the present-day margins
20 of Zealandia. Faults trending NE-SW and E-W are parallel to the mid-ocean ridge separating
21 Southern Zealandia and western Antarctica, ~800-1000 km from the Canterbury Basin, while NW-
22 SE rift faults are sub-parallel to the spreading centre between Australia and Northern Zealandia.

23 Sub-parallelism between spreading centres and rift faulting is consistent with a model in which the
 24 multiple directions of extension produced mild (<20%) distributed stretching associated with the
 25 embryonic stages of Gondwana breakup. We argue that normal faulting in southeastern Zealandia
 26 relates to the plate-tectonic forces responsible for Gondwana fragmentation, starting ~20 Myr
 27 before continental breakup and subsequent formation of mid-ocean ridges. With the onset of
 28 seafloor spreading, extension became localised along the spreading centres and stretching of crustal
 29 blocks distal (>500 km) from these centres ceased or continued at much diminished rates.

30

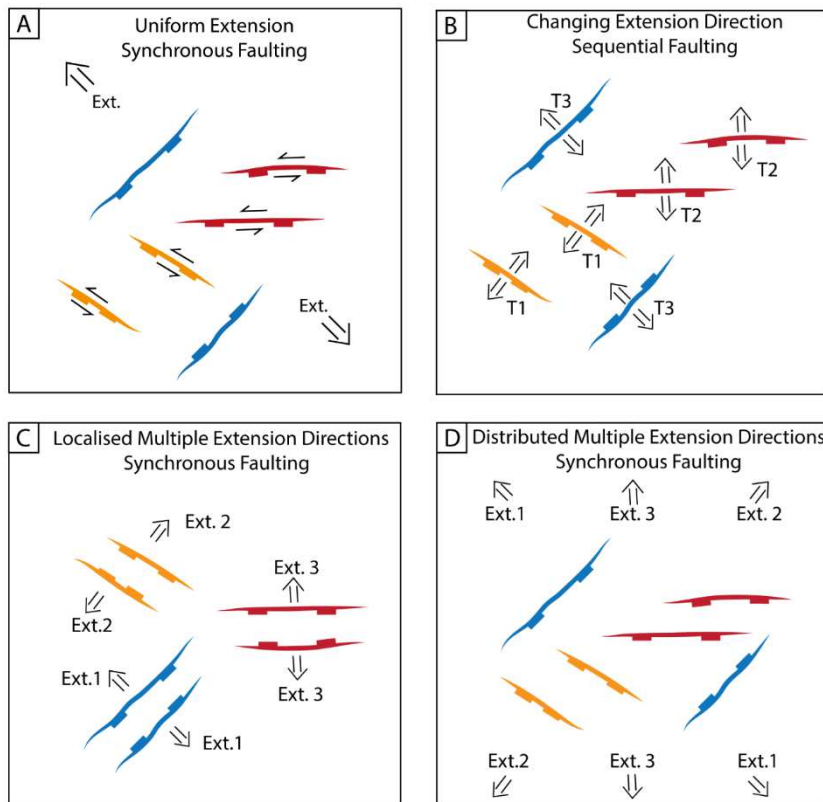
31 Keywords: New Zealand; south Zealandia; Canterbury Basin; rift faults; multi-directional
 32 extension; fault kinematics.

33

34 **1. Introduction:**

35 Rift systems are the surface expression of crustal thinning and mantle convection, typically
 36 accommodating >20% stretching ($\beta=1.2$) over time periods of 5 to 20 Myr (Davison and Underhill,
 37 2012). Extension can be confined to 10-100 km wide rift valleys or distributed across rift provinces
 38 that can be >1000 km wide (Ravnås and Steel, 1998). Rifting may produce complex fault
 39 geometries controlled by orthogonal or oblique extension and pre-rift zones of weakness within
 40 basement rocks (e.g. Morley et al., 2004; Philippon et al., 2015; Morley, 2017). Displacements on
 41 rift faults vary from dip-slip to strike-slip, depending on the obliquity of the fault to the regional
 42 stretching direction (Fig. 1A – e.g. Ring et al., 1994; Morley et al., 2004; Philippon et al., 2015).
 43 Stretching directions can vary with time, resulting in changes of fault kinematics, or in the creation
 44 of new sets of rift faults oriented obliquely to the original rift faults (Fig. 1B – e.g. Morley, 2017).
 45 Conversely, at rift triple junctions, stretching directions may change spatially with near pure
 46 extension on synchronous rift systems that trend at high angles (e.g., 30-90°) to each other (Fig. 1C
 47 - e.g. Jurassic North Sea rift system, Coward et al., 2003; Zanella et al., 2003; Late Cretaceous

48 Southern Atlantic rift system, Heine et al., 2013; African rift system, Mohr, 1970; Koptev et al.,
49 2018). Outside these triple junctions, tectonic normal faults (i.e. excluding non-tectonic fault
50 systems such as polygonal faults), formed due to multiple directions of synchronous extension are
51 rare and the processes leading to their formation poorly understood (Fig. 1D).



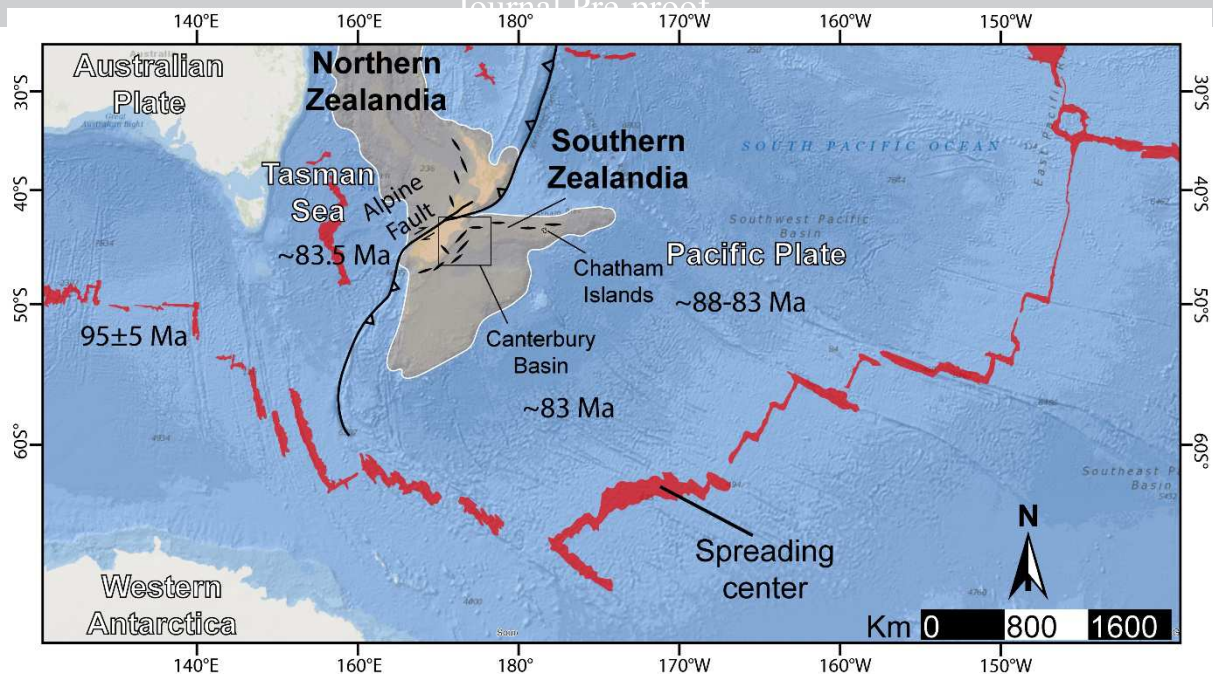
52

53 **Figure 1** Sketch showing four scenarios accounting for the presence of the NE-SW (blue polygons),
54 E-W (red polygons) and NW-SE (orange polygons) rift faults in the Canterbury Basin: (A)
55 Synchronous faulting with uniform extension (Ext. plus arrows represent the regional direction of
56 extension). (B) Sequential faulting with changing extension direction through time (Tn represents
57 different rifting events at different orientations). (C) Localised multiple extension directions with
58 synchronous faulting (e.g. Triple Junctions) (Ext. plus arrows represent different stretching
59 directions). (D) Synchronous faulting with multiple directions of extension (Ext. plus arrows
60 represent different stretching directions).

61 In this paper, we study multiple directions of synchronous extension using normal faults that
62 vary in strike in Southern Zealandia, east of New Zealand's South Island. These faults are part of

63 the large Late Cretaceous Rift Province (> 4 million km 2) that covered much of the Zealandia
64 continent (Mortimer et al., 2017) and produced several Mesozoic-Cenozoic rift basins (Fig. 3A -
65 e.g. Laird and Bradshaw, 2004; Strogen et al., 2017). Extension produced NE-SW, E-W and NW-
66 SE striking fault sets in the Canterbury Basin region (Figs. 2 and 3 - Field and Browne, 1989;
67 Browne et al., 2012; Jongens et al., 2012; Sahoo et al., 2014). These fault sets all accommodate a
68 component of normal displacement and have been assumed to have formed at different times due to
69 changing tectonic processes and extension directions (as in Fig. 1B - Tulloch et al., 2019). The non-
70 coeval hypothesis for the formation of different fault sets may be favoured because it is considered
71 the most parsimonious explanation for their formation. For example, Tulloch et al. (2019) propose
72 multiple phases of rifting in Southern Zealandia with faults trending 130°, 90° and 70° forming at
73 98 to 95 Ma, 90 Ma and 89-82 Ma, respectively. Alternatively, all fault sets could have accumulated
74 displacement synchronously, perhaps associated with NW-SE extension, so that E-W and NW-SE
75 trending fault sets carried significant components of strike-slip (as in Fig. 1A). Finally, and
76 considered the least likely explanation, each of the main fault sets may have formed synchronously
77 and accrued mainly dip-slip movement to produce multiple directions of coeval extension in the
78 continental crust of southeastern Zealandia (as in Fig. 1D). Discriminating between these alternative
79 hypotheses has important implications for Gondwana continental breakup processes and requires a
80 combination of fault kinematic and timing information.

81



82

83 **Figure 2** Regional bathymetric map showing the location of spreading centres (red polygons)
 84 surrounding Zealandia (brown polygon) as defined by crustal thickness (Mortimer et al., 2017).
 85 Ages displayed along the spreading centers correspond to the age of the oldest oceanic crust from
 86 Storey (1995); Müller et al. (2000); Laird and Bradshaw (2004); Wright et al. (2016) and Rieftahl
 87 et al.(2020). Short black lines on Zealandia correspond to the main orientation of Albian-Santonian
 88 (~105-83 Ma) rift basins formed within Zealandia Late Cretaceous rift province (Strogen et al.,
 89 2017).

90 Despite extensive studies of rift evolution in the Canterbury Basin during the Cretaceous,
 91 the timing and kinematics of the different fault sets is poorly constrained (Field and Browne, 1989;
 92 Browne et al., 2012; Jongens et al., 2012; Sahoo et al., 2014). Three sets of rift faults crop-out
 93 onshore, but structural analysis of the syn-rift phase is not possible due to Cenozoic compression,
 94 inversion and erosion associated with formation of the current plate boundary (i.e. the Alpine fault)
 95 between the Pacific and Australian plates (Browne et al., 2012; Jongens et al., 2012). In contrast,
 96 offshore parts of the basin did not experience significant contraction or strike-slip displacement
 97 during the Cenozoic (Fig. 5 - Field and Browne, 1989; Browne et al., 2012; Jongens et al., 2012;
 98 Barnes et al., 2016). Therefore, the offshore Canterbury Basin presents an opportunity to observe

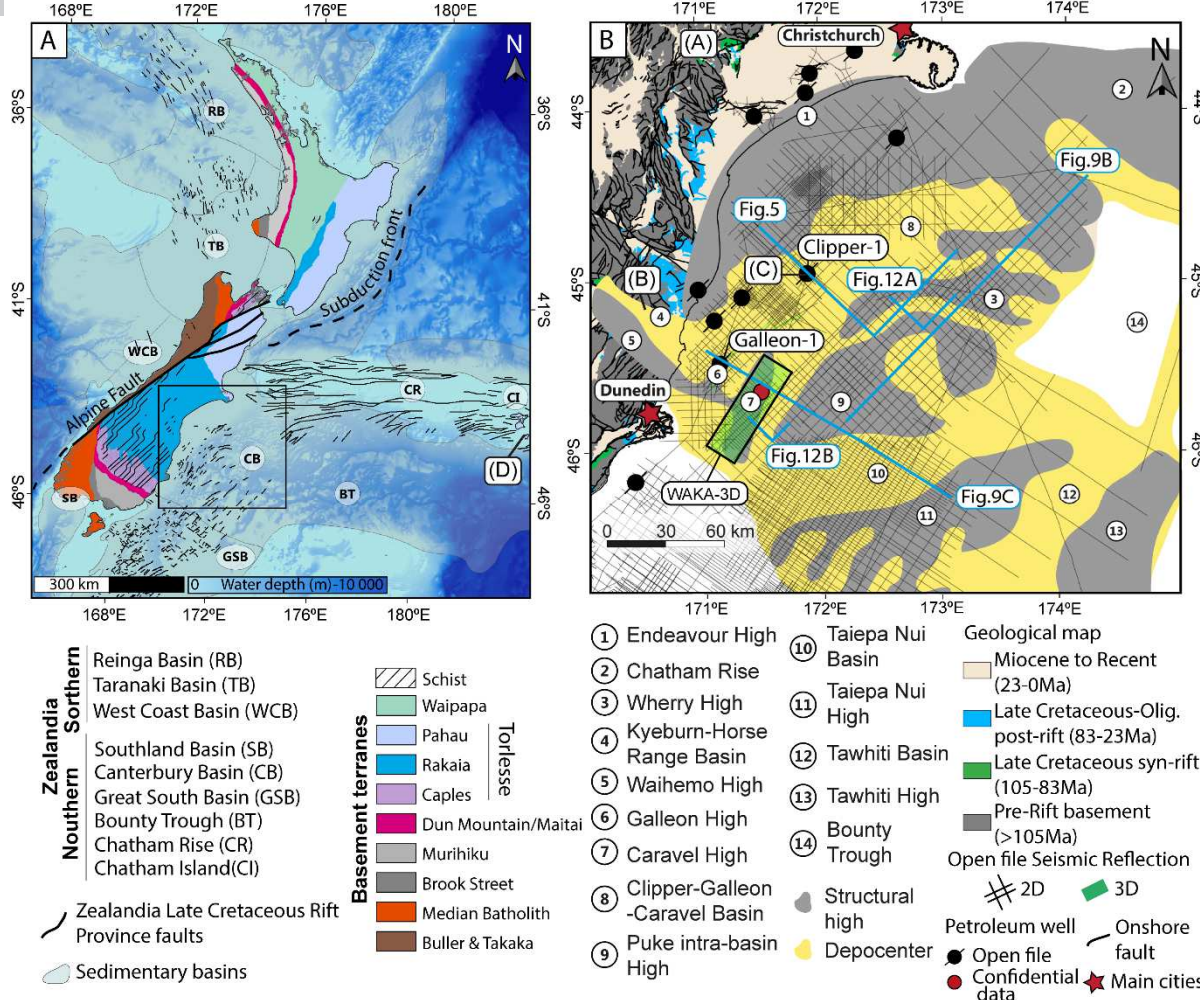
99 undeformed Late Mesozoic to Cenozoic strata that illuminate Gondwana deformation both prior to
 100 and following breakup.

101 Here we present a model in which Cretaceous stretching of Zealandia was driven by
 102 Gondwana breakup, with analysis of faulting providing a basis for a deeper understanding of this
 103 process. We primarily use 2D seismic reflection lines from the offshore Canterbury Basin in
 104 southeastern Gondwana to determine the first-order timing, geometries and kinematics of each of
 105 the three fault sets. With these data we examine whether the different fault sets were coeval and if
 106 they primarily accommodated normal displacement or a mix of dip-slip and strike-slip dependent on
 107 their orientations. Our structural analysis has implications for the early low-strain stages of crustal
 108 stretching in Zealandia that ultimately led to continental breakup with eastern Gondwana. The data
 109 suggest that the three main fault sets primarily accrued normal dip-slip producing synchronous
 110 multi-directional extension (as in Fig. 1D). We propose that multi-directional continental rifting
 111 across Zealandia, prior to continental breakup, reflects extension directions perpendicular to the
 112 future spreading centers that vary in trend $> 90^\circ$ and now bound Zealandia continental crust (Fig.
 113 2). The results may have application throughout Zealandia and elsewhere along other rifted margins
 114 which enclose blocks of continental crust.

115

116 **2. Geological Setting**

117 Extension of eastern Gondwana during the Late Cretaceous (~105-85 Ma) initiated the
 118 formation of eight main sedimentary basins throughout Zealandia (Figs. 3A - e.g. King et al., 1999;
 119 Laird and Bradshaw, 2004; Strogen et al., 2017). These rift basins developed parallel to both
 120 seafloor spreading centres and basement structural fabrics (Figs. 2 and 3A). The resulting Zealandia
 121 continental crust is largely submerged (~94% beneath water) as are many of the sedimentary basins
 122 (including the Canterbury Basin) that mainly rest on Mesozoic basement (Fig. 3 – Mortimer et al.,
 123 2017).



124

125 **Figure 3** (A) New Zealand base map showing onshore basement terranes, offshore Late Cretaceous
 126 faults and associated sedimentary basins (adapted from Mortimer, 2004; Arnot et al., 2016; Sahoo
 127 et al., 2017). (B) Base map of the Canterbury Basin showing locations of figures, key localities,
 128 seismic lines, wells, and structural highs and lows (derived from Field and Browne, 1989; Sahoo et
 129 al., 2015). Names 8-13 have been introduced by Barrier (2019). In the text, rift faults are identified
 130 by the horst and depocentre they separate. (A), (B), (C) and (D) corresponds to the position of the
 131 stratigraphic sections present in Figure 4.

132

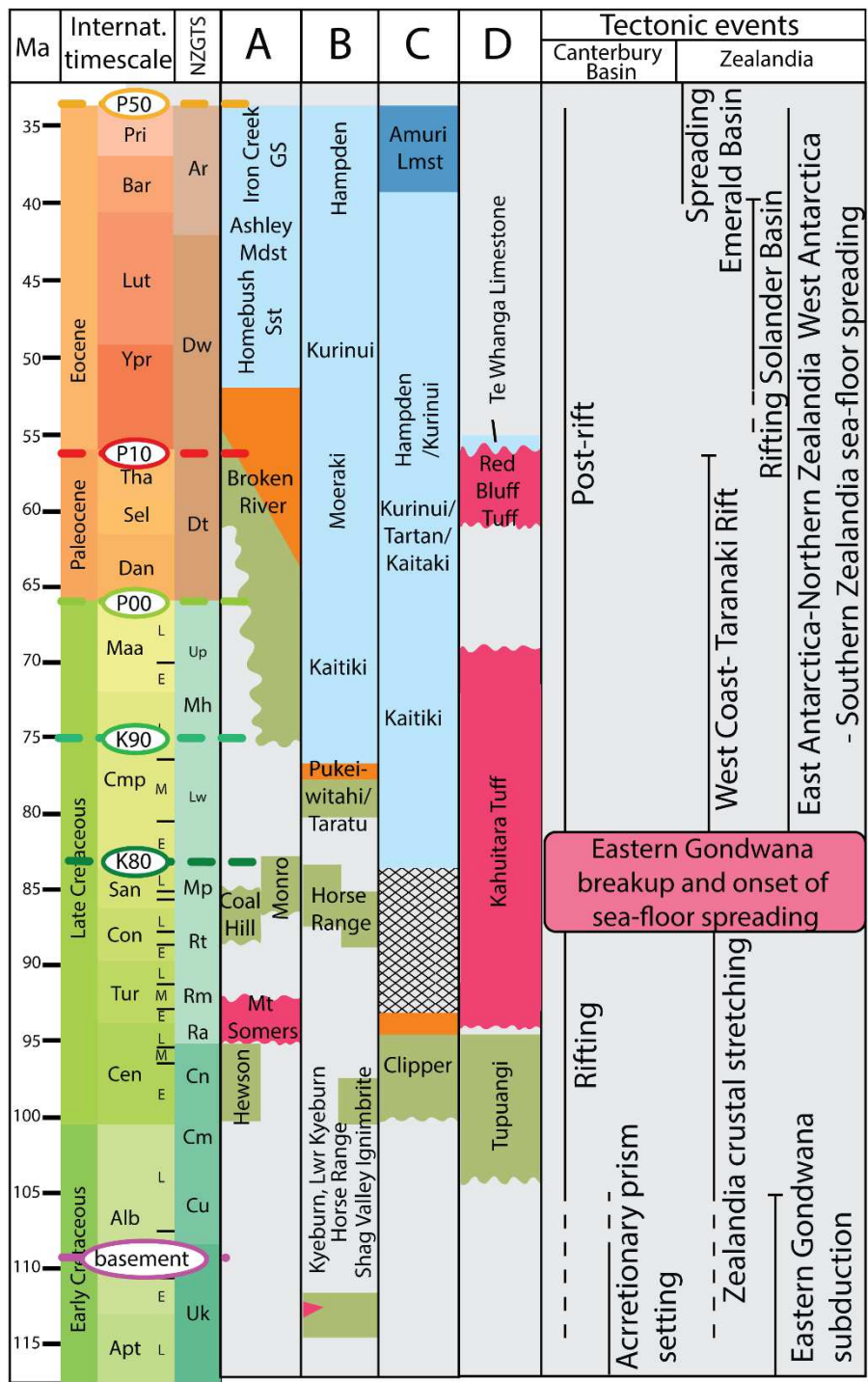
133 The Canterbury Basin in southeastern Zealandia comprises Cretaceous extensional faults with
 134 throws <6 km, reflecting the syn- and post-rift tectono-sedimentary evolution of Zealandia (Figs. 3,
 135 4 and 5 – Field and Browne, 1989; King et al., 1999). Crustal stretching resulted in a series of

136 horsts, grabens and half grabens in three main structural domains (Figs. 3B and 5). The first of these
 137 domains is referred to as the Clipper domain (after Field and Browne, 1989) and comprises mainly
 138 NE-SW striking faults, parallel to the mid-ocean ridge between Southern Zealandia and western
 139 Antarctica (Fig. 2 and 3B). The second domain corresponds to the North Otago domain, comprising
 140 NW-SE striking faults (e.g., the onshore Waihemo Fault) (Fig. 3B - Bishop, 1974; Bishop et al.,
 141 1976). The third domain corresponds to the Chatham Rise domain characterized by E-W trending
 142 faults (Fig. 3 - Wood et al., 1989; Wood and Herzer, 1993). The Chatham Rise domain extends at
 143 least as far east as the Chatham Islands, which are located ~800 km west from the onshore
 144 Canterbury Basin. Some outcrops and onshore seismic reflection profiles record both NE-SW and
 145 E-W rift faults of Late Cretaceous age in the central and western onshore Canterbury Basin
 146 (Browne et al., 2012; Jongens et al., 2012).

147 Rifting followed the cessation of Mesozoic subduction along eastern Gondwana at ~105 Ma,
 148 and immediately preceded seafloor spreading at ~85 Ma (Fig. 4 - Sutherland, 1999; Laird and
 149 Bradshaw, 2004; Davy, 2014; Adams et al., 2017; Strogen et al., 2017; Higgs et al., 2019).
 150 Subduction is inferred to have ceased following collision between the Chatham Rise and the
 151 Hikurangi Plateau, a thickened section of oceanic crust, at ~105 Ma prior to the formation of the
 152 normal faults examined in this paper (Laird and Bradshaw, 2004; Davy, 2014; Crampton et al.,
 153 2019). Canterbury Basin basement terranes may have played a role in the formation and geometry
 154 of some E-W and NW-SE striking Cretaceous normal faults. These basement terranes formed part
 155 of the accretionary prism of a Permian-Early Cretaceous subduction system along eastern
 156 Gondwana (Figs. 3A and 5 - Laird, 1993; Mortimer et al., 1999; Laird and Bradshaw, 2004;
 157 Mortimer, 2004, Mortimer et al., 2014). The terrane boundaries and structures form zones of
 158 weakness which, in some cases, could have been reactivated during rifting (Barrier, 2019; Tulloch
 159 et al., 2019).

160 Onshore strata in the Canterbury Basin support the view that normal faulting and crustal
 161 stretching closely followed the cessation of subduction (Tulloch et al., 2009; Adams et al., 2017;

162 Strogen et al., 2017). Onshore syn-rift formations in the Canterbury Basin typically display upward
163 fining non-marine successions, comprising alluvial fan to fluvial conglomerate, sandstone, siltstone,
164 mudstone and coal, overlain by marine transgressive sediments (Field and Browne, 1989). Onshore,
165 syn-rift strata are exposed along NE-SW (Western Canterbury Basin), E-W (Chatham Island) and
166 NW-SE (Kyeburn) rift depocenters with ages spanning from ~103 to 83 Ma (Figs. 3 and 4 - Adams
167 and Raine, 1988; Field and Browne, 1989; Wood and Anderson, 1989; Browne et al., 2013).
168 Offshore, only the Clipper-1 exploration well intersects syn-rift strata (Figs. 3B, 4 and 5). The well
169 records a fluvial to paralic syn-rift sequence (~103-93 Ma) overlain by outer-shelf post-rift strata
170 (83-75 Ma), suggesting erosion and/or a hiatus in sedimentation of up to 10 Myr between the syn-
171 rift and post-rift successions (Fig. 4 - Schiøler and Raine, 2011). Laird and Bradshaw (2004)
172 identified two breaks in the syn-rift sedimentary records of Zealandia. The first break occurred in
173 most of eastern Zealandia and was late Coniacian to early Santonian in age (~88-85 Ma). The
174 second break was more regional with a maximum Santonian age. The syn-rift hiatus at Clipper-1
175 could comprise both breaks in the syn-rift sequence. The oldest inferred ages for the rift sequence
176 are from detrital zircon U-Pb dating of silicic tuff layers at Kyeburn in the onshore Canterbury
177 Basin of 112.5 ± 0.2 to 114 ± 2 Ma (Tulloch et al., 2009; Adams et al., 2017). It is not clear, however,
178 whether these tuff beds were deposited within, or below, syn-rift growth strata and the timing of
179 faulting relative to the formation of the tuff is equivocal (Bishop et al., 1976; Mitchell et al., 2009).
180 Therefore, for the purposes of this study we adopt an age of ~105 Ma for the onset of rifting which
181 is consistent with the conclusions of other workers (e.g. Strogen et al., 2017).



182

183 **Figure 4** Stratigraphic charts for the Canterbury Basin (modified after Strogen et al., 2017)
184 summarizing the main seismic horizon nomenclature used in this study and the major tectonic
185 processes active in the Canterbury Basin and Zealandia from the Early Cretaceous (~117 Ma) to the
186 base Oligocene (~34 Ma). The four stratigraphic sections correspond to (A) the western onshore
187 Canterbury Basin, (B) the southern onshore Canterbury Basin and (C) Clipper-1 exploration well

188 which is the only offshore well to intersect the syn-rift succession and (D) North Pitt Island in the
 189 Chatham Islands (for locations see Fig. 3).

190 The post-rift phase of Canterbury Basin sedimentation commenced with the onset of eastern
 191 Gondwana breakup at ~85 Ma (Figs. 4 and 5 - Adams et al., 2017; Strogen et al., 2017; Higgs et al.,
 192 2019), and the formation of new oceanic crust between Zealandia, Antarctica and Australia (e.g.
 193 Grindley and Davey, 1982; Laird, 1993; Sutherland, 1999; Laird and Bradshaw, 2004). The onset of
 194 seafloor spreading between Zealandia and eastern Gondwana is generally thought to have occurred
 195 between 88-83 Ma (Figs. 2 and 4 - e.g. Grindley and Davey, 1982; Laird, 1993; Storey et al., 1995;
 196 Sutherland, 1999; Müller et al., 2000; Laird and Bradshaw, 2004; Wright et al., 2016; Rieftahl et
 197 al., 2020). Following the onset of seafloor spreading in southeastern Gondwana, the tectonic
 198 activity decreased significantly in the Canterbury region for >40 Ma (Figs. 4 and 5). Indeed, after
 199 ~85 Ma, only minor displacements (<250 m throws) accrued on some normal faults prior to the
 200 Oligocene (Field and Browne, 1989; Sahoo et al., 2015). Therefore, we refer to this minor late-stage
 201 normal faulting, occurring post onset of seafloor spreading (~85 Ma), as the post-rift phase. This
 202 tectonic phase was mainly followed by the initiation of the present-day transpressive plate boundary
 203 west of the Canterbury Basin, namely the Alpine Fault, during the Late Eocene to Miocene (Fig. 3A
 204 - Field and Browne, 1989; King, 2000; Stagpoole and Nicol, 2008; Barrier et al., 2019; Strogen et
 205 al., 2019). Offshore Cenozoic deformation in the Canterbury region may have produced minor
 206 inversion ratios (<0.10) on some Cretaceous faults within ~50 km of the coastline, however, as this
 207 inversion covers <20% of the basin and does not impact our general conclusions.

208 **FIGURE 5 HERE (FILE SOURCE>10 MB)**

209 **Figure 5** (A) Uninterpreted (top) and interpreted (bottom) composite seismic reflection profile tied
 210 to the Clipper-1 well showing rift geometries in the offshore Canterbury Basin. Syn-rift (Green) and
 211 post-rift (yellow) tectonic units are displayed on the interpreted seismic profile. Note that some of

212 the main rift faults display minor (<250 ms TWT, <~250 m) post-rift displacement. See Figure 3B
 213 for locations.

214

215 **3. Methods and Data**

216 **3.1. Seismic Mapping**

217 We have mapped faults using ~26 000 line kilometres of 2D seismic reflection profiles and one
 218 3D seismic reflection survey. The seismic reflection data were acquired between 1966 and 2014 and
 219 accessed here via the New Zealand Petroleum and Minerals (NZPAM) 2015-2018 data packs (Fig.
 220 3B). We interpreted seismic reflection lines over an area of ~160 000 km². The quality and
 221 coverage of the seismic data are variable, with the number and spacing of seismic lines decreasing
 222 eastwards, hampering horizon and structural interpretation. The average line spacing in the study
 223 area is typically about 5-10 km, therefore faults with lengths <10 km may have not been sampled.

224 We have interpreted six seismic horizons in the basin and refer to these horizons using the
 225 “K” and “P” naming convention established by GNS Science (Figs. 4 and 5 - Strogen and King,
 226 2014). Seismic data have been tied to the most recent biostratigraphic ages for strata from five
 227 petroleum exploration wells in the offshore Canterbury Basin (Schiøler and Raine, 2011). Absolute
 228 horizon ages were primarily assigned using the International and New Zealand Geological Time
 229 Scales (Cooper et al., 2004; Raine et al., 2015). The list of seismic horizons interpreted is presented
 230 in Table 1.

231 **Table 1** List of horizons interpreted in this study with the various nomenclature used.

Color code	Horizon Name	GNS Science nomenclature (Strogen & King, 2014)	Age (Ma)	NZ Stage	International Stage
—	Top Eocene	P50	34	Runangan	Priabonian
—	Top Paleocene	P10	56	Teurian	Thanetian
—	Top Late Cretaceous post-rift	P00	66	upper Haumurian	Maastrichtian
—	Intra Late Cretaceous post-rift	K90	78	lower Haumurian	intra Campanian
—	Top Late Cretaceous syn-rift	K80	~85	Piripuan	Santonian
—	Top Basement	basement	~105	Urutawan to Korangan	Aptian-Albian

232

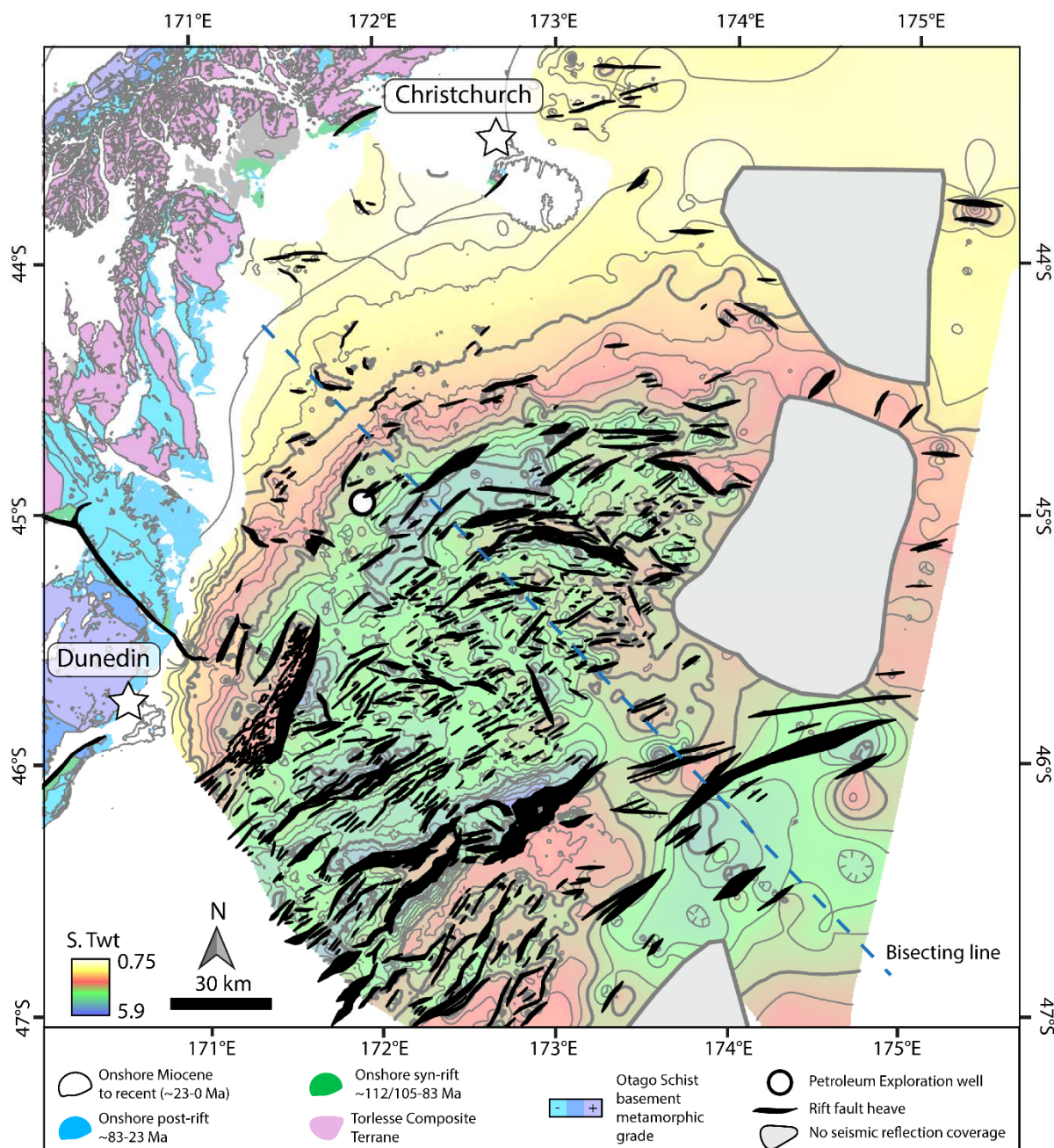
233 Clipper-1 well in the offshore Canterbury Basin penetrated Cretaceous syn-rift strata (Figs.

234 4 and 5 - Schiøler and Raine, 2011). The base of the syn-rift succession (offshore inferred to be
 235 ~105 Ma) is the early Albian unconformity between the top basement reflector and growth strata
 236 (for further details see Barrier, 2019). We tied the top of syn-rift reflector (Santonian - K80) to the
 237 Clipper-1 well and used this tie to constrain our interpretation throughout the study area by mapping
 238 growth strata geometries (as opposed to the draping geometries that are more typical of post-
 239 breakup reflector packages above the Santonian or K80 reflector). The Santonian (K80) reflector
 240 also marks the onset of spreading along the mid-ocean ridges surrounding Zealandia (Barrier,
 241 2019). No syn-rift horizons nor breakup sequence could be mapped across the basin. The lack of
 242 correlation between fault-controlled and disconnected depocentres and the poor age control of syn-
 243 rift strata from wells precludes detailed analysis of fault growth.

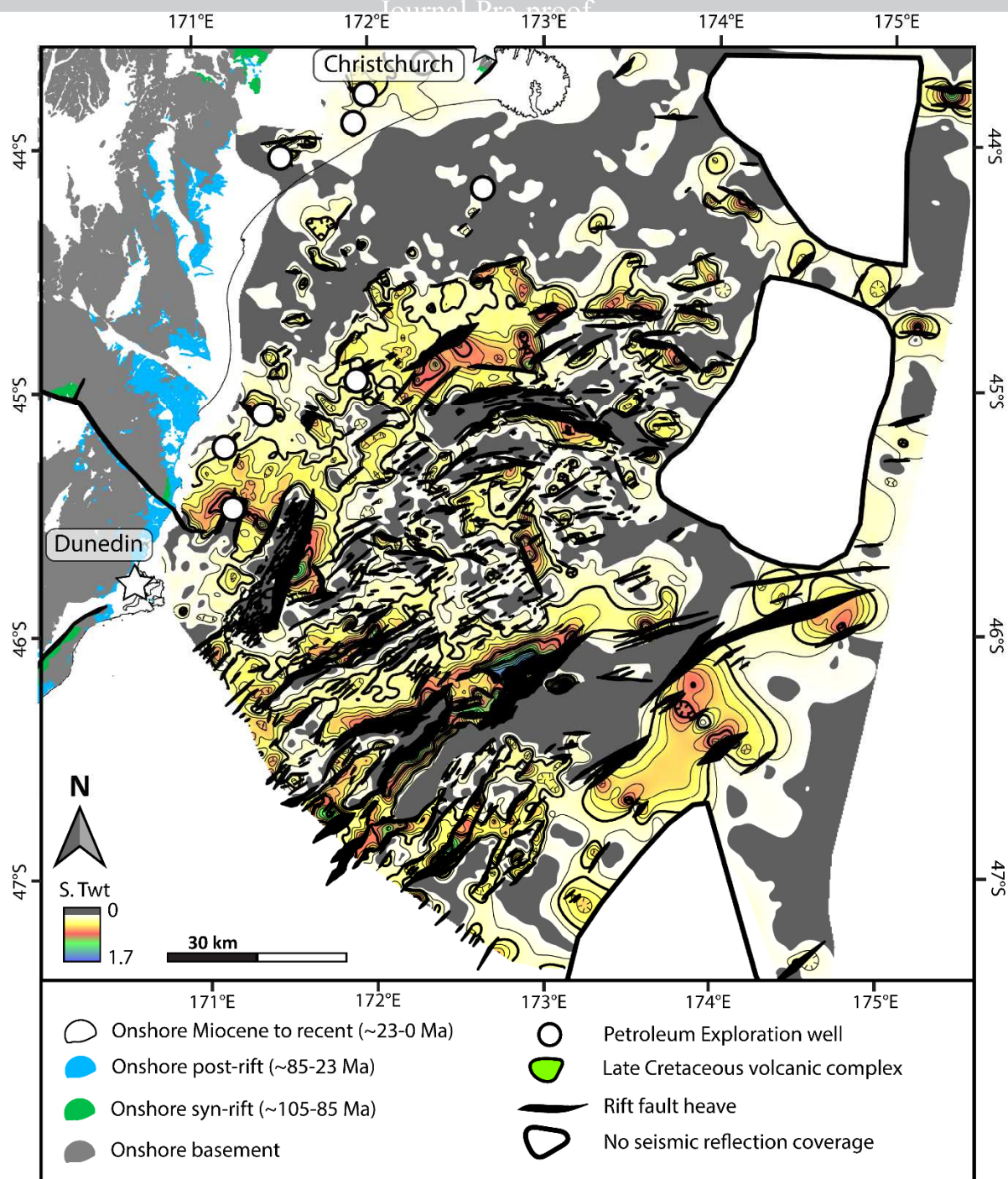
244

We generated isochron grids with structural contours and associated faults for the top
 245 basement (Fig. 6), the syn-rift early Albian to Santonian interval (Fig. 7 - ~105 to 85 Ma; basement
 246 to K80; Urutawan-Piripauan New Zealand stages), and the post-rift intra-Campanian to
 247 Maastrichtian interval (Fig. 8 - ~85 to 66 Ma; K80-P00; Haumurian New Zealand stages). We used
 248 these maps to show the locations and geometries of faults active during rifting. Our three isochron
 249 maps define a number of depocenters and structural highs for which we adopted names from the
 250 literature (Fig. 3B - Field and Browne, 1989; Barrier, 2019). The main rift faults of the Canterbury
 251 Basin are named after the horst blocks and the depocenters that they bound or separate.

252



255 **Figure 6** Top of Basement isochron structural map of the offshore Canterbury Basin with fault
 256 polygons displaying rift fault heaves. Blue dashed line separates northern and southern areas (see
 257 text for further discussion).

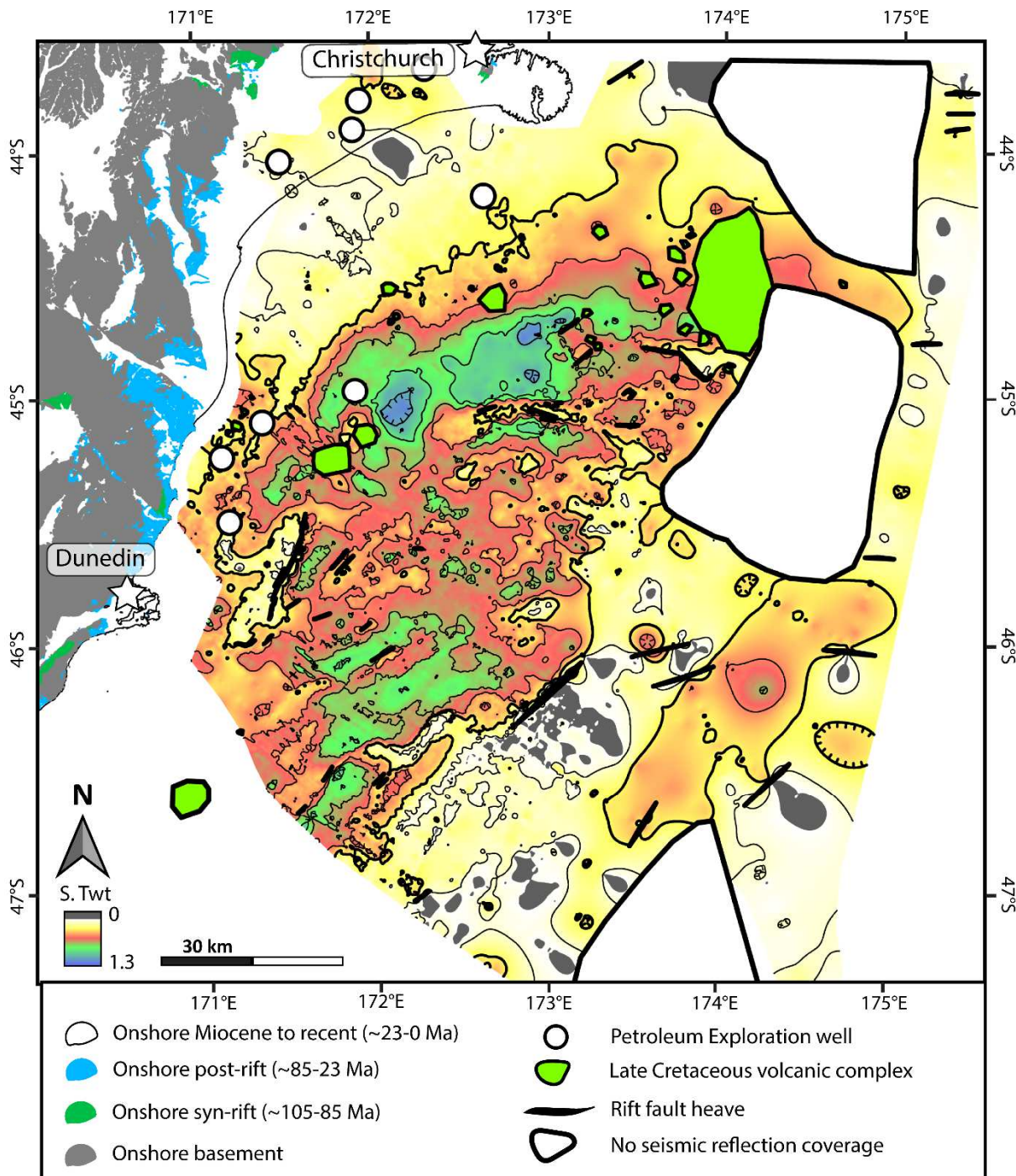


258

259 **Figure 7** Syn-rift mid-Cretaceous (~105-85 Ma) isochron structural map showing the locations of
 260 depocenters and horst structures. Fault heave is represented by thickness of black polygons which is

261

proportional to the total syn-rift fault heave.



262

263 **Figure 8** Syn-rift mid-Cretaceous (~105-85 Ma) isochron structural map showing the locations of
 264 depocenters and horst structures. Fault heave is represented by thickness of black polygons which is
 265 proportional to the total syn-rift fault heave. (C) Post-rift Late Cretaceous (~85-66 Ma) structural
 266 isochron structural map showing the decrease in rift fault activity post-breakup of eastern
 267 Gondwana.

3.2. Fault measurements

269 Our top basement and syn-rift (early Albian-Santonian interval, ~105 to 85 Ma, Urutawan to
270 Piripuan New Zealand stages) isochron structural maps show the geometry of faults with a
271 component of normal displacement (Figs. 6,7 and 8). We have measured maximum vertical
272 displacements (i.e. throws) for the top basement to Eocene horizons. As the changes in
273 displacement due to depth conversion and compaction is generally <20% (e.g. Taylor et al., 2008),
274 depth conversion and decompaction of syn-rift growth packages was not performed to derive the
275 first-order displacements presented here. Where syn-rift early Albian-Santonian (K80) reflectors
276 were not present on the footwall of a fault, we measured the throw between the top basement in the
277 footwall and the top basement or syn-rift horizons in the hangingwall. The resulting displacement
278 measurements are minimums as basement and syn-rift strata in the fault footwalls could have been
279 eroded. For six faults, we measured throws on multiple seismic lines (with spacing of 4-10 km)
280 along the length of each trace and used these to generate horizon separation diagrams for
281 displacements that accumulated during rifting. In cases where small throws (< 250 ms TwT, <~250
282 m) post-date rifting we subtracted these displacements from the top basement displacement to
283 derive total values for syn-rift faulting.

284 We measured fault lengths for all mapped faults in the seismic reflection dataset. In the majority
285 of cases, the measured fault lengths are minimum values which are impacted to varying degrees by
286 the seismic resolution and by the seismic line spacing (e.g., 2D vs 3D). Three-dimensional seismic
287 reflection datasets typically resolve shorter faults and have small absolute errors on the estimated
288 lengths (e.g. Watterson et al., 1996; Meyer et al., 2002). Our comparison of 3D and 2D seismic
289 data, presented in section 4, demonstrates the impact of data quality on fault length measurements
290 for this study. For the 2D dataset mainly used in our study, we expect underestimates in fault
291 lengths of kilometres and under-sampling of the numbers of faults with lengths of up to ~20 km. To
292 decrease the influence of seismic line spacing on measured fault lengths, where possible we

293 projected fault traces beyond their last observed seismic line using observed decreases in throw
 294 towards the tip.

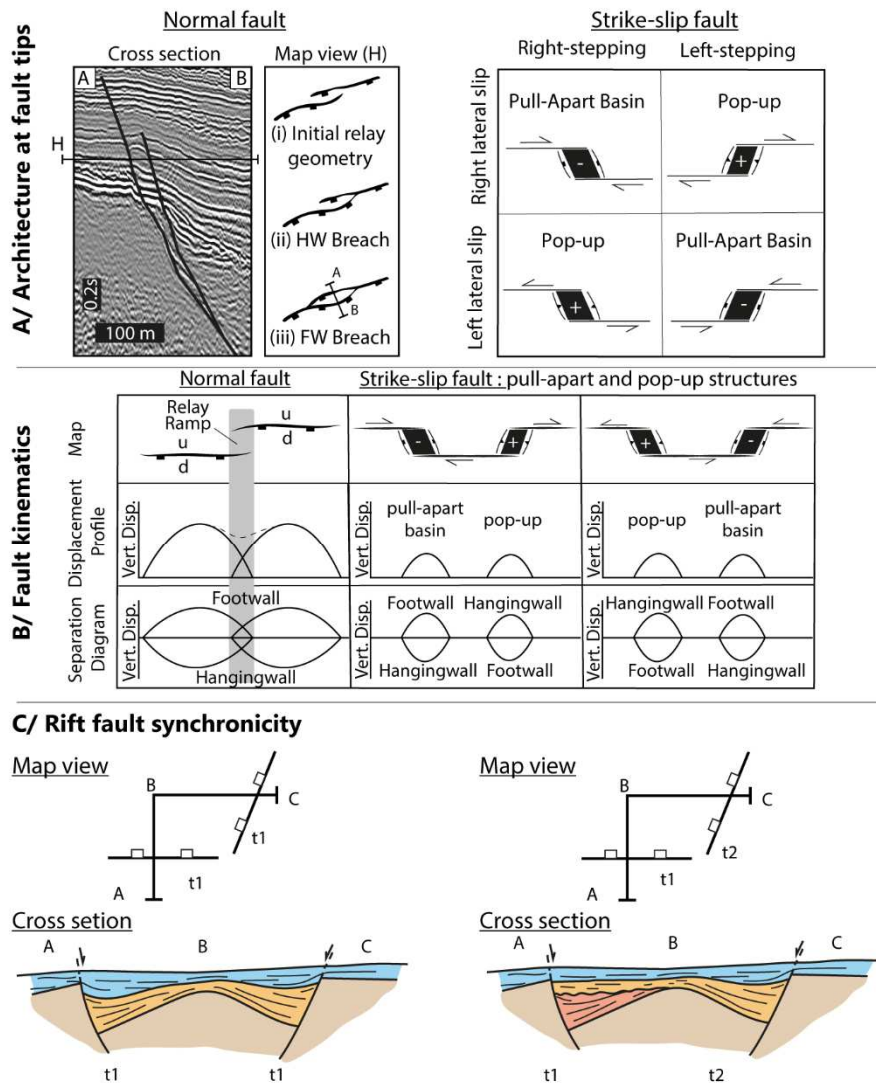
295 We calculated fault dips in seismic sections assuming that the faults are planar, using the heave
 296 and throw for depth-converted sections. Given uncertainties in the detailed seismic velocities in the
 297 Canterbury Basin, due to poor well penetration within the syn-rift interval, time to depth conversion
 298 was completed using velocities of between 3 km/s and 5 km/s. We then applied apparent dip
 299 corrections for the faults that did not intersect the seismic profiles at an angle of 90° to calculate the
 300 true fault dip. These calculations provide first-order estimates of fault dip and could under-estimate
 301 the true dip due to footwall erosion and errors picking the horizon cut-offs.

302 We use three parameters to analyse the kinematics and displacement histories of the different
 303 trends of rift faults (Fig. 9). First, average fault trends ($N=654$) were measured from line segments
 304 connecting the mapped tips of fault traces. We plotted the trends of these line segments in bi-
 305 directional rose diagrams (Figs. 10A and 10B). For curved faults that display segments varying in
 306 strike from NE to E, we measured the trend of individual segments. Different fault trends were
 307 observed in the northern and southern sub-areas of the offshore Canterbury Basin (Fig. 10),
 308 separated by a line that forms the boundary between mainly NE-SW and E-W fault trends (Fig. 6,
 309 blue dashed line).

310 Second, we estimate the kinematics of the different fault sets, and differentiate between dip-slip
 311 and strike-slip displacements, by analysing vertical displacements represented by horizon separation
 312 diagrams across segment boundaries and along the entire lengths of faults (Figs. 9A and 9B). In the
 313 case of mainly dip-slip (normal) movement, the area of overlap between two fault segments will
 314 display a relay ramp or breached relay-ramp geometry across which fault displacements often
 315 decrease and a deficit in throw is accommodated by bed rotations and sub-seismic faults (e.g. Walsh
 316 et al., 1999; Childs et al., 2017; Nicol et al., 2020). In contrast, for strike-slip faults, segmentation
 317 produces pull-apart basins, releasing bends and pop-up structures across which locally high vertical

318 displacements can be observed (Fig. 9A - e.g. Zampieri et al., 2003; Morley et al., 2004; Massironi
319 et al., 2014). These strike-slip faults would be expected to have both a reverse and normal sense of
320 displacement along their length, with the slip sense being dependent on the sense of fault stepping
321 (e.g. Morley et al., 2004). Such horizon separation geometries for strike-slip faults will differ from
322 those of predominantly normal faults for which footwall and hangingwall horizons define
323 displacements that rise to a maximum (often near the fault centre) producing symmetrical bell-
324 shaped profiles (Fig 9B). Therefore, vertical displacement profiles across segment boundaries offer
325 an opportunity to identify strike-slip faulting. Horizon separation diagrams for oblique-slip faults
326 may display a combination of geometries as depicted in Figure 9B. However, given the wide
327 variation in fault set orientations, we would expect at least one of these fault sets to have
328 accommodated significant strike-slip if the regional extension direction was uniform and faulting
329 coeval.

330 Third, we determined the relative timing of displacements for each of the three fault sets
331 using syn-rift isopachs and growth strata imaged on composite seismic lines that cross two different
332 fault sets (set out in Fig. 9C). The composite lines enabled the relative timing of displacement on
333 each fault set to be determined by correlating growth strata between fault-related depocentres, with
334 the absolute ages of these growth strata estimated by correlation of seismic reflectors to the Clipper-
335 1 well (see section 3.1).

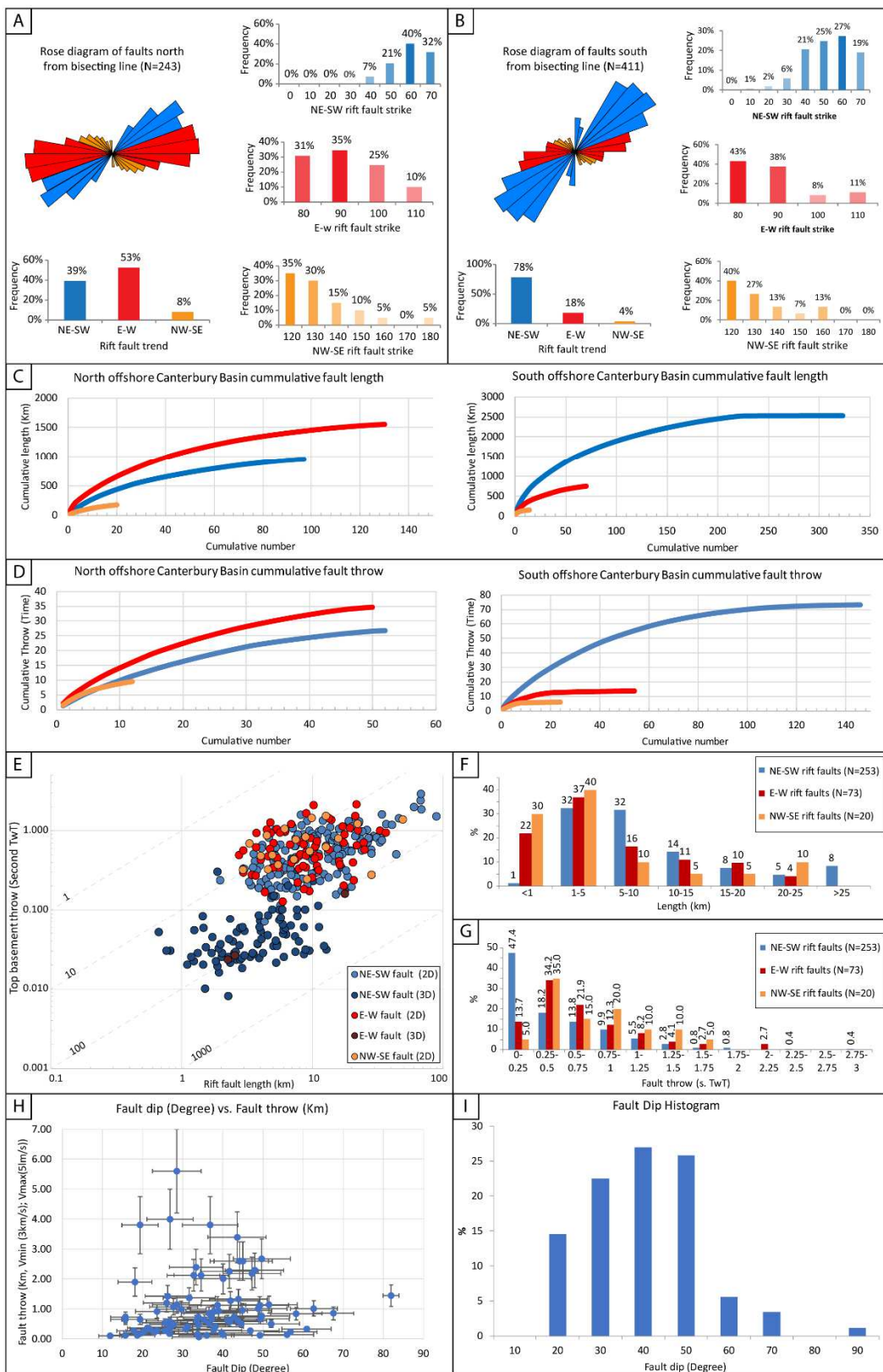


336

337 **Figure 9** (A) Dip-slip or oblique slip movements have been discriminated using rift fault
 338 architecture. For purely normal displacement, fault architecture displays relay and breach
 339 geometries. HW breach: Hangingwall breach; FW breach: Footwall breach (adapted from Walsh et
 340 al., 1999). In the case of strike-slip movement, faults display pop-up or pull-apart basin geometries
 341 (adapted from Massironi et al., 2014). (B) Displacement separation diagrams can be used to
 342 discriminate fault movements. For purely normal displacement, the separation diagram will display
 343 a symmetrical bell-shaped geometry. For oblique motion with both normal and strike-slip
 344 displacement, the separation diagram will display a horizontal offset of the bell-shaped curves. Note
 345 that the footwall throw measured does not represent a maximum value due to erosion and therefore
 346 smoothing of the relief. (C) Summary of the parameters used to determine the timing of rift faults.

348 **4. Quantitative fault analysis**349 **4.1 Fault geometries and lengths**

350 We have mapped 654 faults on seismic reflection profiles with vertical displacements of 70
351 to 2880 ms two way time (TwT) (<100 m to ~5 km) and lengths of 0.6 - 90 km for the top basement
352 and syn-rift horizons (NB the onshore Kyeburn fault is estimated to have a throw of ~4-5 km,
353 making it potentially the largest fault in the basin, see Barrier, 2019). The largest faults in the
354 system that we interpreted (here referred to as border faults) are segmented or form single traces
355 which bound symmetrical grabens and asymmetric half-grabens (Figs 5, 6, 7 and 11). Faults
356 typically display a range of fault strike, dip direction, and dip angle (~30 to 70°) (Figs. 6 and 10). In
357 the region of study, we recognise two main fault sets that strike NE-SW and E-W, with a subsidiary
358 fault set that strikes NW-SE (Figs 6 and 10). NE-SW faults range in trend from 10° to 70° with the
359 majority of traces trending between 50° and 70° (Figs. 10A and 10B). This fault set is present
360 throughout the Canterbury Basin, and dominates the fault system in the southeast part of the basin
361 (Figs. 6 and 12). These faults are approximately parallel to the southeastern margin of Zealandia
362 and to the oceanic ridge (and associated spreading centre) that separates Zealandia from western
363 Antarctica (Fig. 2). E-W to WNW-ESE faults most often trend from 70° to 110° (Figs. 10A and
364 10B). They are most commonly located on the Chatham Rise and onshore west of the Rise, where
365 they are parallel to the trend of the Rise and the former Mesozoic subduction margin (Figs. 3 and 6).
366 NW-SE trending faults range in trend from 110° to 160° and are subordinate to NE-SW and E-W
367 sets (Figs. 10A and 10B). NW-SE faults are most common in the southern Canterbury Basin and
368 include the Waihemo Fault, which is parallel to basement terrane boundaries, including the Rakaia
369 Terrane and Otago Schist boundary (Figs. 3 and 6 - Mortimer 1993; Mortimer 2000; Deckert et al.,
370 2002).



371

372 **Figure 10** Analysis of the differences north and south of the bisecting line (see Figure 6) for the
 373 offshore Canterbury Basin between (A) rift fault trends to the north, (B) fault trends to the south,
 374 (C) fault lengths and (D) fault throws. (E) Graph showing the relationship between rift fault length

375 and maximum vertical displacement. Graph shows weak linear correlation due to a difference in
 376 measurement precision between faults interpreted on 2D and 3D seismic datasets. (F) Histogram of
 377 rift fault length categorized into fault trends (NE-SW, E-W and NW-SE) showing an approximate
 378 log-normal distribution centred on the 1-5km fault length. (G) Histogram of rift fault throws
 379 categorized into fault trends (NE-SW, E-W and NW-SE). Note that the high number of NE-SW
 380 faults with throw <0.25 second TwT results due to a higher fault sampling from the Waka 3D
 381 seismic survey that covers a major NE-SW rift fault. (H) Graph showing the fault dip and the fault
 382 throw of rift faults measured along a selection of cross sections. (I) Histogram showing the
 383 distribution of fault dip.

384 Our mapping shows that NW-SE and NE-SW faults can occur in similar parts of the basin
 385 and form abutting relationships, but no cross-cutting faults have been mapped (Figs. 12 and 11). In
 386 contrast, E-W trending faults are mainly present in the northern part of the Canterbury Basin, with
 387 the faults progressively changing in orientation from NE-SW to E-W approaching the E-W
 388 Chatham Rise. The change in predominant fault trend from NE-SW to E-W occurs across a NW-SE
 389 trending line (Fig. 6, blue dashed line). Some individual faults cross this line and have different
 390 trends along their length. For example, the fault bounding the southern edge of the Wherry High
 391 comprises three right stepping segments (Figs. 3B, 6, 7 and 13). The trend of the three segments
 392 changes from NE-SW to E-W and to NW-SE along ~90km (Figs. 6, 7 and 13). In this case,
 393 progressive rotation of the dominant trend of the fault is achieved by a series of small discrete
 394 changes across segment boundaries.

395 **FIGURE 11 HERE (FILE SOURCE>10 MB)**

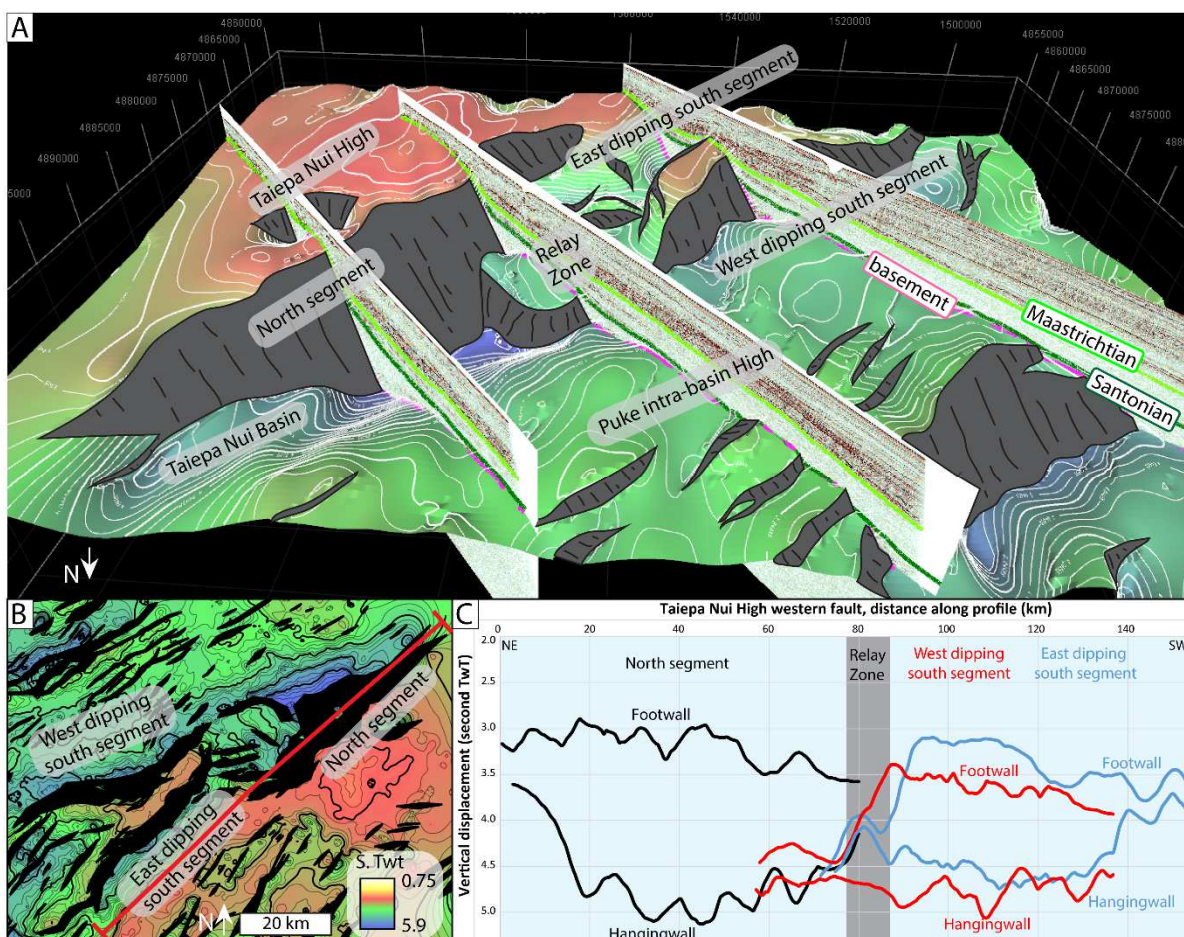
396 **Figure 11** (A) N-S and (B) E-W composite seismic profile sections showing rift depocenters and
 397 structural highs together with Late Cretaceous syn-rift and Late Cretaceous to Eocene post-rift
 398 sequences. Note that some of the main rift faults display minor (<250 ms TwT, <~250 m) post-rift
 399 displacement. See Figure 3B for locations.

401 **4.2 Fault kinematics**

402 Constraining fault kinematics is key to understanding the origins of Cretaceous faults in the
403 Canterbury Basin. These faults universally display a component of normal dip-slip, with the
404 available seismic reflection data providing little evidence of strike-slip (Figs. 5 and 11). We have
405 analysed fault geometries and displacements in the form of displacement length plots and horizon
406 separation diagrams to test the hypothesis that one or more of the fault sets accommodated a
407 component of strike-slip (Figs. 12C and 13C). The plot of fault length against throw in Figure 8E
408 shows a broad correlation for NE-SW and E-W fault sets. NW-SE trending faults are generally
409 shorter for a given maximum displacement, but also have lower displacements than the two other
410 sets. For both northern and southern offshore Canterbury Basin, the fault category displaying the
411 greatest lengths also displays the highest throws (Fig. 10C and 10D). In addition, we observe that
412 NW-SE faults are less common in the basin compared to the other fault sets, in some cases possibly
413 because these faults are parallel to the primary seismic line orientation. Therefore, despite
414 differences in the sampling and numbers of faults in each set, the fault length and displacement
415 (throw) relationships are similar and do not support the possibility of mainly strike-slip motion
416 along one of the rift fault sets.

417 Analysis of horizon separation diagrams for two faults with segments oriented NE-SW, E-W
418 and NW-SE (i.e. each of the orientations for the three fault sets) also shows no unequivocal
419 evidence for strike-slip. Our mapping shows that the Taiepa Nui Fault trends NE-SW, dips ~30-60°
420 to the NW, and contains a large right-stepping overlap zone (~20 km wide) between the northern
421 and southern segments of the fault (Figs. 12A and 12B). Within the overlap zone, the top basement
422 seismic horizon is displaced by faults that traverse the zone of overlap between segment tips, and
423 connect the primary northern segment to two southern segments (Figs. 12A and 12B). We observe
424 that vertical displacements on the main fault segments decrease across the overlap zone, which

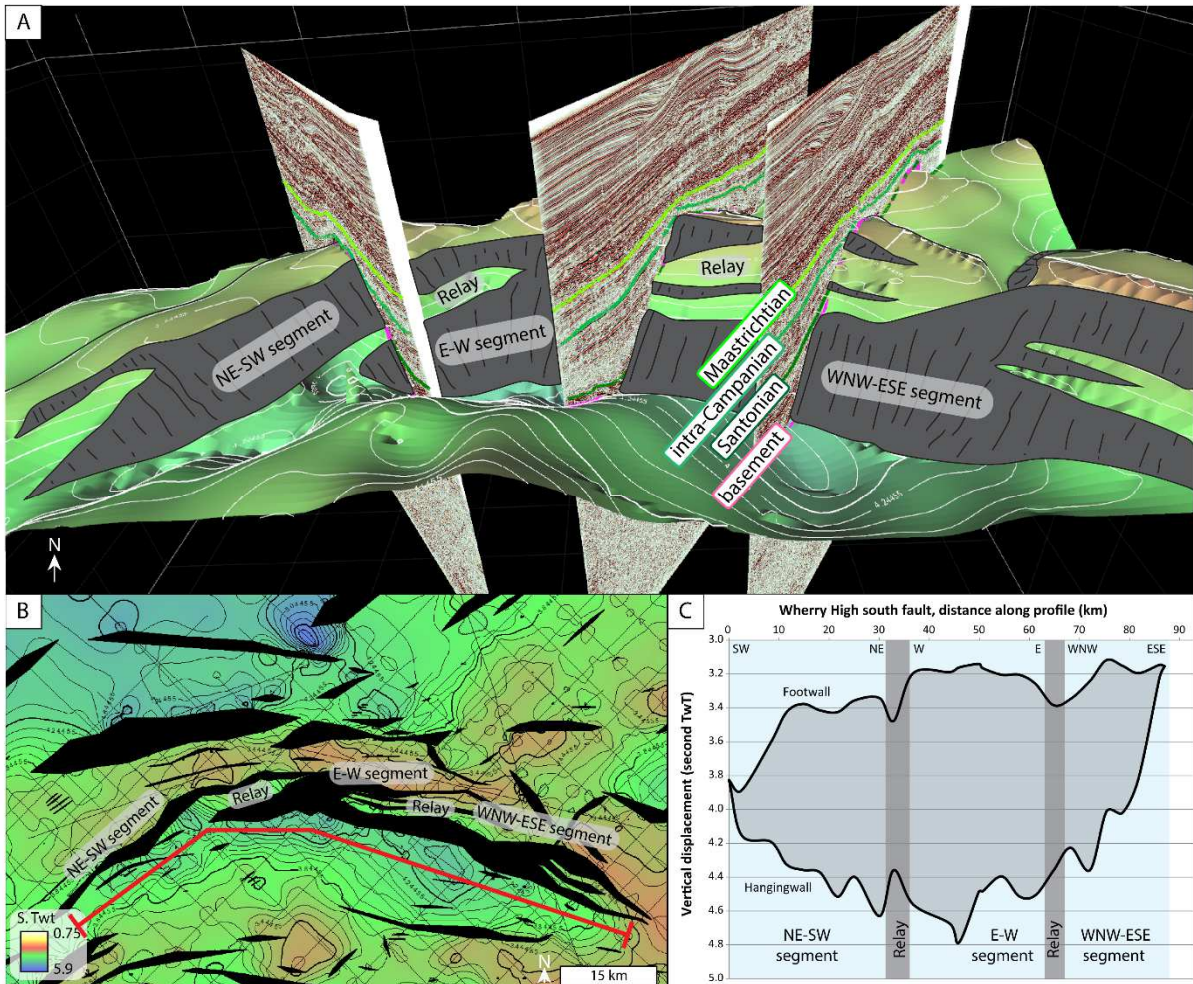
425 appears to facilitate the transfer of vertical displacement between segments (Fig. 12C). We interpret
 426 that the geometry and displacement of the segmentation and overlap zone are characteristic of
 427 normal faults separated by a relay ramp and accruing predominantly dip-slip displacement (e.g.
 428 Childs et al., 1995, 2017; Morley, 2017; Nicol et al., 2020). If the normal fault and relay ramp
 429 interpretation is correct, then the NE-SW striking Taiepa Nui Fault primarily accommodated NW-
 430 SE extension orthogonal to the strike of the fault.



431
 432 **Figure 12** (A) 3D view of the top of basement grid along the NE-SW rift fault bounding the
 433 western edge of the Taiepa Nui High (location on Figure 3B). Faults show a ramp structure typical
 434 of dip-slip movement. (B) Top of basement isochron map showing the geometry fault segments on
 435 the western side of the Taiepa Nui High. Red line represents the position of the separation diagram
 436 on which horizons and associated throws for each fault segment. (C) Separation diagram along NE-

437 SW Taiepa Nui Rift faults displaying complementary changes in displacement across the overlap
 438 zone, consistent with dip-slip faults.

439 To further examine the fault kinematics, we also conducted vertical displacement analysis on
 440 the fault bounding the southern edge of the Wherry High, which comprises three segments that dip
 441 ~30-70° S to SE, strike NE-SW, E-W and NW-SE, separated by overlap zones <2 km wide (Figs.
 442 13A and 13B). We suggest that if the faults were accruing slip in association with a regional NW-
 443 SE extension direction (as interpreted for the Taiepa Nui Fault), E-W faults would be expected to
 444 accommodate left-lateral strike-slip with right-stepping overlap zones forming pop-up structures.
 445 Instead, we observe that for all fault orientations, the overlap zones have geometries consistent with
 446 breached relays (Figs. 13A and 13B) and interpret the entire fault to have mainly accommodated
 447 normal dip-slip. To test the dip-slip hypothesis we generated a horizon separation diagram for the
 448 entire length of the Wherry High south fault (Fig. 13C). The horizon separation diagram for the
 449 Wherry High south fault shows hangingwall and footwall top basement horizon geometries, with
 450 the greatest throw located towards the centre of the fault. These displacements do not indicate that
 451 the normal displacement decreases on E-W or NW-SE sections of the fault as might be inferred if
 452 these parts of the fault accommodated significant strike-slip (Fig. 13C). In addition, the separation
 453 diagram shows decreases in throw at the segment boundaries which is inconsistent with these
 454 overlap zones forming pop-up structures (Fig. 13C). Instead, displacement lows at overlap zones
 455 can be explained if these zones form relay ramps on normal faults, where the displacement lows
 456 reflect ramp rotation and small-scale faulting in the overlap zone (cf., Childs et al., 1995).
 457 Therefore, we conclude that the Wherry High south fault is mainly dip-slip along each of the three
 458 segments despite their variable strikes.



459

460 **Figure 13** (A) 3D view of the top of basement surface along the Wherry Fault south of the Wherry
 461 High (location on Figure 3B) with three fault segments of three different orientations (NE-SW, E-W
 462 and NW-SE) linked via overlap zones. (B) Top of basement isochron map showing the geometry
 463 and nomenclature of the different segments of the Wherry Fault. Red line represents the position of
 464 the separation diagram on which throws of each fault segments are projected. (C) Separation
 465 diagram along the Wherry Fault displaying a bell-shaped geometry typical of dip-slip movement.
 466 The decrease in displacement around 32 km and 65 km reflect relay ramps between the different
 467 segments of the fault.

468 If our interpretations of the separation diagrams are correct, then E-W and NE-SW trending
 469 faults primarily formed in association with N-S and NW-SE extension, respectively. The amount of
 470 extension accommodated by faulting across the basin and perpendicular to each fault set is modest
 471 (<20%). We have calculated extension by comparing initial and final bed lengths or areas (e.g. E=

472 (Li-Lf)/Li, where E is the amount of extension either expressed as a percentage or as a Beta factor
 473 (β), Li is the initial length, and Lf is the final length). For the area calculation across the entire study
 474 area, the ratio between the total fault heave area to the total mapped area produces a stretching of
 475 ~11% ($\beta=1.11$). We also estimated the extension from two composite seismic sections, one oriented
 476 E-W in the southern offshore Canterbury Basin, intersecting mostly NE-SW faults, and a second
 477 one oriented N-S, intersecting mostly E-W rift faults (Fig. 11). The E-W composite section returned
 478 an extension of 16.7% ($\beta=1.167$) and the N-S composite section 11.3% ($\beta=1.113$). Our
 479 measurements suggest that within the study area NE-SW faults accommodate about twice the
 480 extension that E-W faults accommodate, with the values of extension being comparable to many
 481 other rift basins worldwide (stretching <20%, $\beta=1.20$; Davison and Underhill, 2012). As the
 482 amounts of extension are low (<20%) we see no evidence for core complex formation in the study
 483 area.

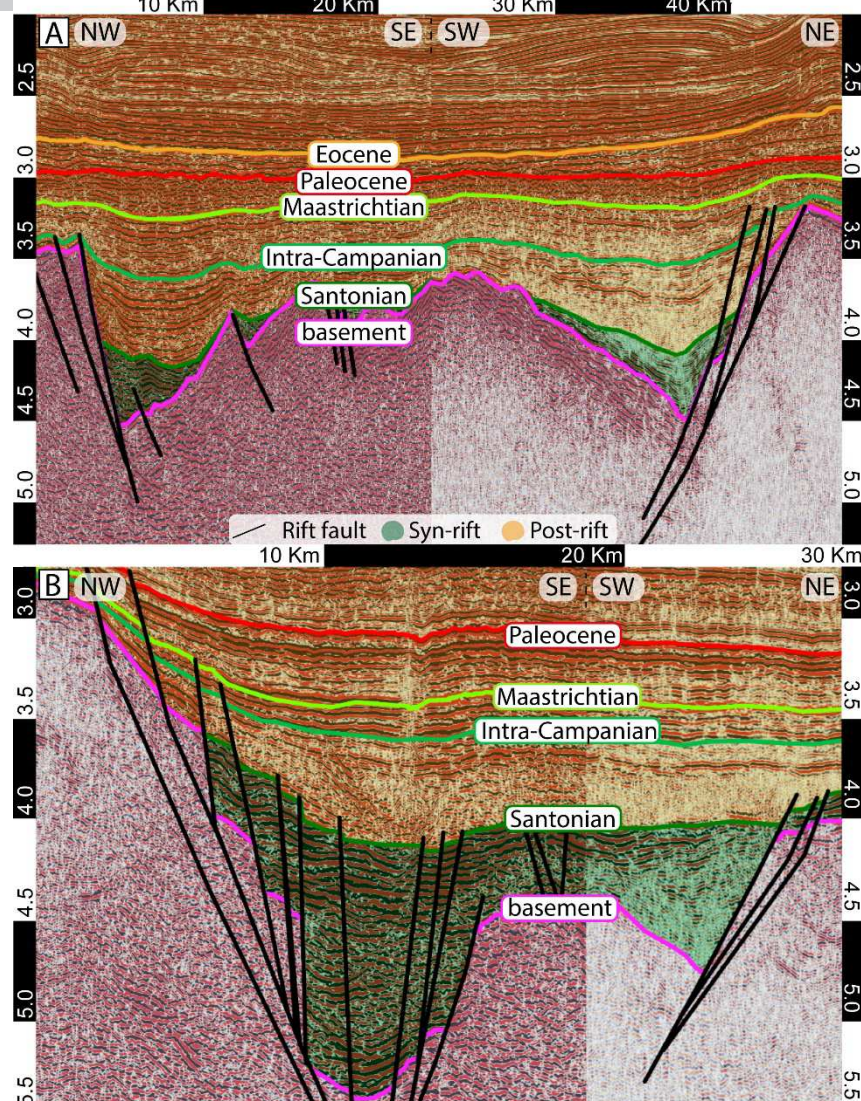
484

485 **5. Timing of faulting**

486 We used the geometries of growth strata adjacent to normal faults with different trends to
 487 examine whether they accrued displacement simultaneously (as in Fig. 1D) or sequentially (as in
 488 Fig. 1B). On a basin-wide scale, we observe that sediment thickness between the top basement to
 489 K80 isochron increases in the hangingwall of each of the main fault sets, suggesting an element of
 490 synchronicity in their displacement histories. To test this idea further we generated composite
 491 seismic lines that each cross two of the three fault sets (e.g. Fig. 14). These composite lines
 492 universally indicate that all fault sets were active synchronously (within the 10 Myr resolution of
 493 the data); here we present two examples. On the Wherry High (Fig. 3B), a composite seismic
 494 reflection cross-section intersects both NE-SW and E-W faults. Because the depocentres associated
 495 with each fault set are under-filled, growth strata are not laterally continuous across the section (Fig.
 496 14A), however, the same Late Cretaceous post-rift reflector package (K90, intra Campanian, ~85 to

497 ~78 Ma) overlies both growth strata packages. Therefore, we interpret the different fault orientations
498 to have been active coevally and to have ceased accruing displacement at about the same time.
499 Although the depocentre geometries in the hangingwall of each fault set are broadly similar, and
500 support a synchronicity argument, the poor age resolution of the basin-fill sequence means that it is
501 possible that displacement accumulation on each fault set was episodic.

502 To further constrain the timing of faulting we constructed a second composite reflection
503 profile across the eastern Caravel High (Fig. 3B) that intersects both NE-SW and NW-SE faults
504 (Fig. 14B). The section displays lateral continuity between growth strata in each fault-controlled
505 depocentre, which is overlain by the same Late Cretaceous post-rift reflector package (K90, intra
506 Campanian, ~85 to 78 Ma) identified in Figure 14A. Therefore, we interpret these two faults to
507 have ceased accruing displacement at about the same time. The timing of the onset of faulting along
508 the margins of the Caravel and Wherry highs are difficult to assess but the geometries of both sets
509 of growth strata are similar and indicate that each fault set probably commenced movement around
510 the same time.



511

512 **Figure 14** (A) Composite seismic reflection profile in the Wherry High region crossing two rift
 513 faults, one oriented NE-SW and the other E-W, showing their approximate synchronicity. (B)
 514 Composite seismic reflection profile adjacent to the Caravel High crossing two rift faults, one
 515 oriented NE-SW and the other NW-SE, showing their synchronicity. See Figure 3B for locations.
 516 Vertical Scale in second two-way time. See supplementary material 1 for un-interpreted sections.

517 Our conclusions based on the seismic interpretations presented in Figure 14 are consistent
 518 with observations from throughout the basin which suggest that all fault sets were broadly active
 519 coevally during the main rifting phase. In addition, on some faults, minor displacements (<~250 m)
 520 accrued after the cessation of rifting at ~85 Ma, with throws of 0.10-0.25 second TwT, 0.11-0.23
 521 second TwT, and 0.07-0.10 second TwT on NE-SW, E-W and NW-SE rift faults, respectively

522 (Figs. 5, 8 and 11). These late-stage displacements are an order of magnitude less than the main
 523 phase of rifting and the origin of these minor displacements is not discussed further here.

524

525 **6. Discussion**

526 **6.1 Coeval multiple extension directions in the Canterbury Basin**

527 Our fault analysis indicates that the Late Cretaceous NE-SW, E-W and NW-SE trending rift
 528 faults in continental crust of the Canterbury Basin formed due to three coeval and non-colinear
 529 stretching directions. Displacement analysis of segmented NE-SW, E-W and NW-SE trending
 530 faults provides no indication of significant strike-slip and is interpreted to be mainly normal dip-
 531 slip. A predominance of dip-slip is consistent with fault dips that range from 20-70° for all three
 532 fault sets. We cannot discount the possibility of some strike-slip along E-W and NW-SE trending
 533 fault sets; however, if present, this strike-slip is not sufficiently large to be recorded at fault-
 534 segment boundaries as pop-up structures or pull-apart basins. Therefore, we conclude that the
 535 Canterbury Basin appears to have experienced extension in three directions, orthogonal to the three
 536 sets of faults, with N-S extension dominating the southern Chatham Rise and NW-SE extension
 537 dominating the southeastern part of the basin. Despite the moderate dips and high displacements
 538 (e.g., >2 km) on some faults, regional extension associated with each fault set is low (<20%).

539 Dating and mapping of growth strata from this study and from the literature indicate that the
 540 three sets of rift faults were coeval. The ages reported from three onshore locations along three
 541 different trends of rift faults suggest that syn-rift sedimentation occurred at least from ~103 to 83
 542 Ma (e.g., western Canterbury, North Otago and Chatham Islands, Bishop, 1974; Bishop et al., 1976;
 543 Field and Browne, 1989; Wood et al., 1989; Wood and Herzer, 1993; Browne et al., 2012; Jongens
 544 et al., 2012). The timing of faulting onshore is comparable with our analysis of offshore seismic
 545 reflection lines and wells. In addition, the interpreted synchronicity of the three fault sets is

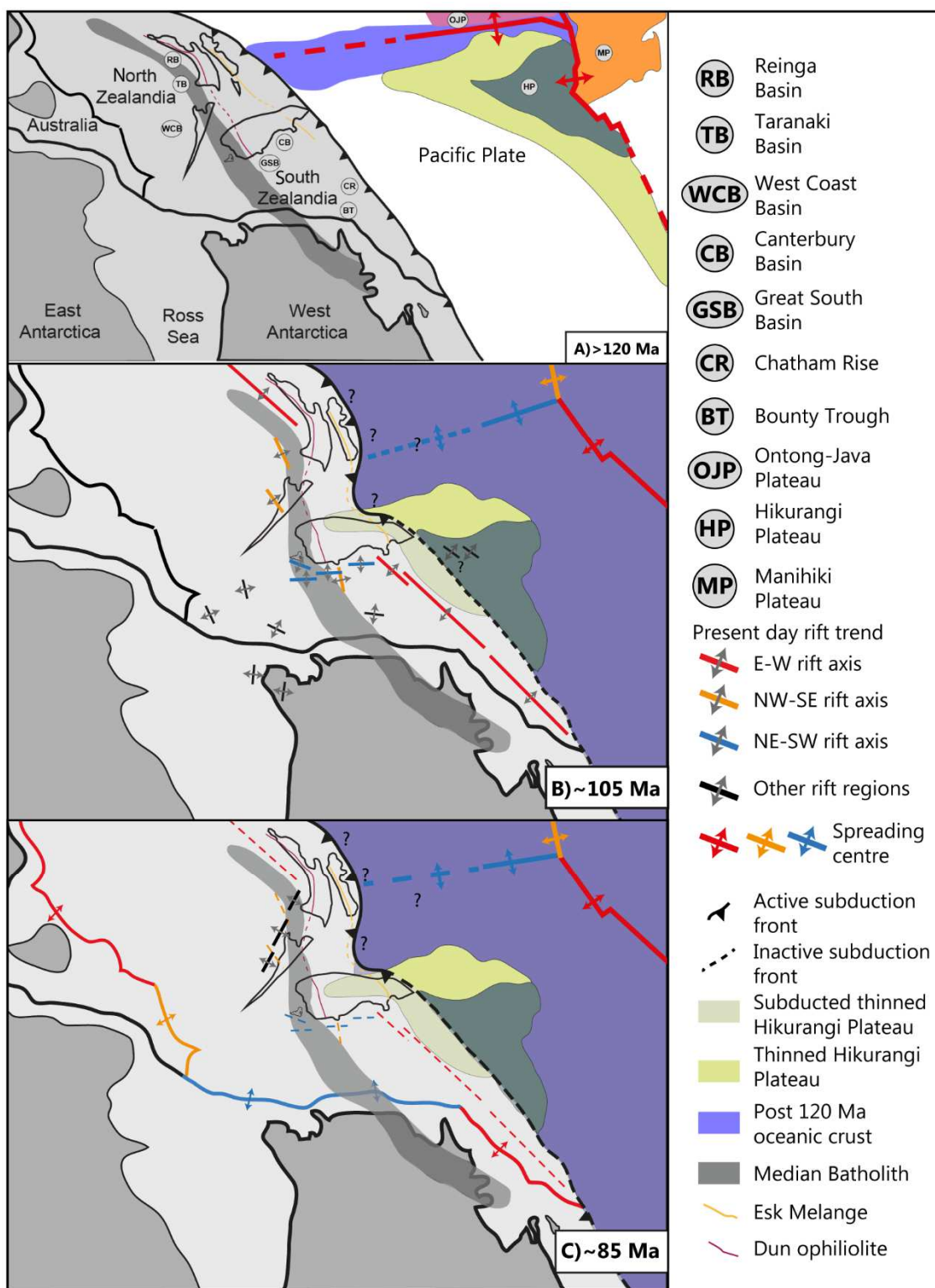
546 consistent with the apparent lack of cross-cutting relationships and strike-slip faulting for these
 547 different sets. Experimental modelling by Henza et al. (2010) suggests that for multiple fault sets
 548 formed sequentially due to changing extension directions, the earlier formed faults are often (>45%)
 549 cross-cut and displaced by later faults. Such cross-cutting relationships are not observed in the
 550 Canterbury Basin. Similarly, Henza et al. (2010) showed some strike slip on later fault sets when
 551 these faults strike at moderate to high angles to each other (e.g., >50°). Therefore, although the
 552 geometries and ages of growth strata from the Canterbury Basin are first-order, comparison of our
 553 results with those of Henza et al. (2010) support the hypothesis that all fault sets in the Canterbury
 554 Basin were active coevally during the main rifting phase.

555

556 **6.2 Implications for Gondwana Continental Breakup**

557 To explore the tectonic drivers for the observed multi-directional coeval extension, we
 558 consider the eastern Gondwana setting of the basin together with intra-basinal factors that could
 559 influence the orientations and kinematics of faulting. We present a series of schematic diagrams
 560 using observations from this paper and the literature to show the evolution of structures along the
 561 eastern Gondwana margin: (A) at ~120 Ma during subduction of the Pacific Plate and prior to onset
 562 of crustal stretching of Zealandia; (B) at ~ 105 Ma during the onset of crustal extension in
 563 Zealandia to show the configuration for the ~20 Myr of distributed extension; and (C) immediately
 564 after the onset of oceanic-crust generation along mid-ocean ridges between Zealandia and eastern
 565 Gondwana (~85 Ma) (Fig. 15). Our data support the view that faults with NE-SW, E-W and NW-
 566 SE trends accommodated extension coevally. Ultimately, such observations provide information on
 567 the embryonic stages of the breakup process distal to the eventual spreading centres, where
 568 continental crust is bounded by spreading centres with a range of orientations (Figs. 2 and 15).
 569 Indeed, sea-floor spreading and the associated mid-ocean ridges vary in orientation around

570 Zealandia and these variations may account for the multiple directions of extension in the
 571 Canterbury Basin (Figs. 2 and 15).



572

573 **Figure 15** Zealandia Cretaceous geodynamic reconstruction during eastern Gondwana breakup
 574 showing the relation between subduction, the formation of Zealandia Late Cretaceous Rift Province

575 and spreading centres defining the margin of Zealandia. (A) Setting prior to the onset of crustal
 576 extension ($> \sim 105$ Ma) showing the geometry of the spreading centres affecting the Pacific plate.
 577 Eastern Gondwana margin is represented in grey colour. (B) Onset of crustal stretching across
 578 Zealandia (~ 105 Ma) showing the distributed extension that took place for ~ 20 Myr prior to
 579 oceanic floor accretion. Local stretching directions are represented by arrows perpendicular to the
 580 rift axis symbols. (C) Reconstruction immediately after the onset of oceanic-crust generation along
 581 mid-ocean ridges (~ 85 Ma). The geodynamic reconstructions are modified from McFadden et al.
 582 (2015), Lamb et al. (2016), Strogen et al. (2017) and Mortimer (2018). Extension affecting the
 583 Hikurangi Plateau from Bland et al. (2015).

584 The NE-SW fault set that dominates the southern Canterbury Basin is roughly parallel to
 585 Southern Zealandia and western Antarctica margins and the associated mid-ocean spreading ridge
 586 which was ~ 500 km east of the study area at the time of mid-ocean ridge inception (blue spreading
 587 centre on Fig. 15C). The NE-SW fault set extends over ~ 900 km continuously to the south into the
 588 Great South Basin where it dominates faulting (Fig. 15B - Sahoo et al., 2015; 2017; Philipps and
 589 McCaffrey, 2019). In addition, the NE-SW fault trend is sub-parallel to the spreading ridge or
 590 transform fault between the Hikurangi Plateau and the Ontong Java Plateau since subducted beneath
 591 Northern Zealandia (blue spreading centre on Fig. 15C - Davy, 2014; Mortimer et al., 2019).
 592 Similarly, the E-W fault set observed in the northern offshore part of the Canterbury Basin extends
 593 ~ 800 km east across the southern Chatham Rise, the Bounty Trough and the southern part of the
 594 Hikurangi Plateau (Fig. 15B - Wood et al., 1989; Wood and Herzer, 1993; Carter and Robert, 1993;
 595 Carter et al., 1994; Bland et al., 2015). This trend is parallel to the Early Cretaceous subduction
 596 margin along the northern edge of the Chatham Rise, parallel to reverse faults and folds interpreted
 597 to have formed during subduction (Barrier, 2019), parallel to the spreading centre that formed
 598 between the eastern end of the Bounty Trough and western Antarctica (red spreading centre on Fig.
 599 15C), and parallel to the spreading centre between the Hikurangi and Manihiki plateaus (red
 600 spreading centre on Fig. 15C), which was likely at least 1000 km north of the Canterbury Basin in

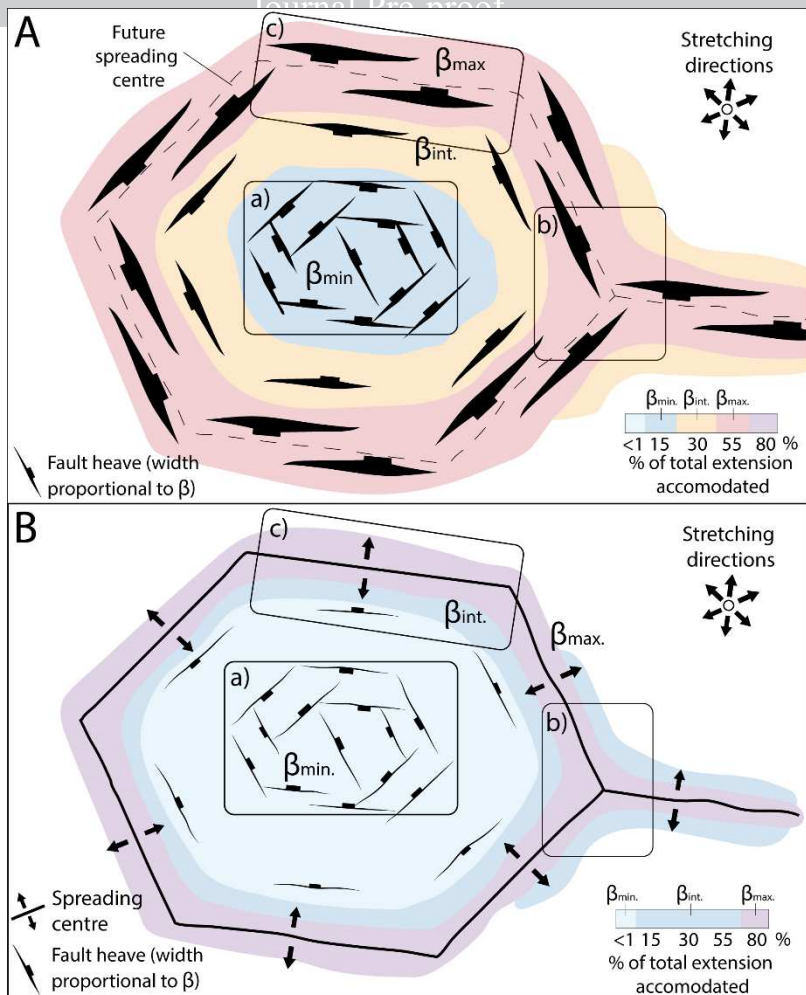
the Late Cretaceous (~105-85 Ma). Last, the NW-SE fault trend is approximately parallel to the spreading centre between Northern Zealandia and Australia (orange spreading centre on Fig. 15C), again despite being located more than 1000 km from the study area, sub parallel to the spreading ridge between the Ontong-Java and Manihiki plateaus (orange spreading centre on Fig. 15C), and sub parallel to basement terrane boundaries exposed onshore (Barrier, 2019).

The E-W and NW-SE fault sets are locally parallel to basement fabric visible on seismic data and it is possible that the locations of these faults were influenced by basement mechanical heterogeneity formed during Mesozoic subduction (Barrier, 2019; Tulloch et al., 2019; Supplementary material 2 and 3). However, both of these fault sets are primarily extensional and appear to accommodate extension normal to far-field spreading centres as would be expected if the extension on faults in Zealandia and along mid-ocean ridges was kinematically related. These favourably oriented zones of weakness in the basement may promote the formation of extensional faults large distances (e.g., >500 km) from the kinematically-related spreading centre.

We hypothesise that the multiple directions of extension observed in the Canterbury Basin were primarily due to far-field stretching imposed on Zealandia prior to eastern Gondwana continental breakup. In our model, changes in the predominant fault set across the Canterbury Basin reflect the changing proximity and influence of future spreading centres on basin faulting (Fig. 15). For example, NE-SW faults predominate in the southern Canterbury and Great South basins which are closest to the west Antarctica Southern Zealandia boundary where it trends NE-SW (Figs. 15B and 15C). The Gondwana breakup model for Cretaceous normal faults may have application across much of Zealandia which also experienced extension prior to the onset of seafloor spreading at ~85 Ma (e.g. Laird and Bradshaw, 2004; Strogen et al., 2017). If this model is correct, then we would expect that Cretaceous normal faults elsewhere in Zealandia were also formed mainly parallel to future breakup mid-ocean ridge systems. To a first-order this appears to be the case with, for example, ~105-85 Ma aged rift faults in northern (Reinga and North Taranaki) and western Zealandia (South Taranaki and West Coast, South Island) trending sub-parallel to Australia-

627 Northern Zealandia and eastern Antarctica-Northern Zealandia spreading centres, respectively
628 (Figs. 15B and 15C). Given the parallelism of the rift faults with the subsequent spreading centres,
629 we suggest that some of the rift structures could have formed as part of the breakup process, which
630 produced a rift province >4000 km long and >1000 km wide distributed across Zealandia, and
631 ultimately led to the separation of Zealandia from eastern Gondwana (Fig. 15B).

632 Coeval multi-directional stretching is widely observed at triple junctions, although we argue
633 that the dimensions of these junction zones (where multi-directional extension may be occurring)
634 are typically smaller than the >100,000 km² of distributed extension in the Canterbury Basin. For
635 example, the North Sea Mesozoic triple junction formed a three-arm rift system where, at the
636 intersection of the rift arms, multiple sets of synchronous rift faults were active (Coward et al.,
637 2003). Distal to the North Sea triple junction zone, only one set of approximately parallel faults can
638 be observed (e.g. Coward et al., 2003). We suggest that in Zealandia stretching differs from triple
639 junctions in that extension occurred in continental crust enclosed, or surrounded by, multiple future
640 spreading centres which varied in trend (Figs. 15 and 16).



641

642 **Figure caption 16** Model of a continental crust affected by multidirectional stretching and
 643 surrounded by future spreading centres illustrating that the faults in the centre of the block are
 644 controlled by the geometries of the margins of the block (e.g., Canterbury Basin). (A) In the time
 645 prior to breakup and seafloor spreading, extension (β) was widely distributed with the percentage of
 646 total extension increasing from the centre outward towards the future spreading centres. (B) In the
 647 time following breakup and seafloor spreading, the locus of extension was focused along the outer
 648 spreading centres whereas the centre was being only moderately stretched. a:Canterbury Basin
 649 model; b Triple Junction model; c Atlantic margin type model.

650 Our work indicates that the initial phase of crustal stretching that preceded Gondwana
 651 breakup was likely characterised by minor (<20%) extension across much of the Zealandia
 652 continental crust. During the crustal stretching phase, between ~105 and 85 Ma, it is not clear how
 653 much extension occurred along the future spreading centres, although we believe that in order to

654 promote the formation of new oceanic crust at these sites it must have been higher (e.g. >80% or
 655 $\beta>1.8$) than the amount of extension that occurred in distal areas such as the Canterbury Basin
 656 (Figs. 15 and 16). The low β factor in the Canterbury Basin may reflect its distal (>500 km) location
 657 relative to future spreading centers. Along the Atlantic margin, for example, where rifting occurred
 658 <300 km from the locus of continental breakup, β values have the potential to be greater (e.g.,
 659 $\beta>1.8$) than those observed in the Canterbury Basin. The long distance (>500 km) of the Canterbury
 660 Basin from the future spreading centers, could account for attenuation of crustal rebound after
 661 breakup in the study area and the apparent absence of a clear lithospheric breakup surface or
 662 breakup sequence in the Canterbury Basin (Fig. 16). Indeed, neither a breakup sequence nor a two
 663 phase breakup has been described along eastern Gondwana, suggesting that this region may differ
 664 from the Atlantic margin or from the South China Sea (e.g., Soares et al., 2012, 2014; Zhao et al.,
 665 2016; Alves and Cunha, 2018; Lei et al., 2019).

666 The duration of the pre-breakup crustal extension distributed across Zealandia likely reflects
 667 the time taken to thin the continental crust sufficiently for the generation of new oceanic crust along
 668 spreading centers. In such cases the duration of extension prior to breakup could be influenced by a
 669 range of factors, including the rates of extension, the thickness of the continental crust, the location
 670 and size of pre-existing structures, and the geothermal structure of the crust (e.g. Dunbar and
 671 Sawyer, 1996; Brune et al., 2016; Salerno et al., 2016; Ulvrova et al., 2019). Whatever the
 672 processes that led to the onset of seafloor spreading around Zealandia, the uniformity in the timing
 673 of this event suggests that these processes may have impacted much of Zealandia.

674 Unlike in the West Coast-Taranaki-Reinga basins, the Canterbury Basin was not subject to a
 675 second phase of rifting which may correspond to either the far-field expression of a transform fault
 676 associated with the Zealandia-western Antarctica oceanic ridge or to a failed rift linked to a triple
 677 junction south of New Zealand (Strogen et al., 2017). Instead in the study area, the onset of seafloor
 678 spreading (~85 Ma) and focusing of extension along the newly created mid-ocean ridge systems
 679 produced a cessation or order-of-magnitude decrease of displacement rates on normal faults (Fig.

680 15C). This focusing of extension along spreading centres may be comparable to the localisation of
 681 strain onto the largest faults in extensional fault systems (Walsh et al., 2001; Meyer et al., 2002).

682 An important implication of the rift systems in this study is that the orientations of mid-
 683 oceanic ridges and the associated extension direction may have been established 10s of millions of
 684 years before the onset of seafloor spreading. The multi-directional stretching and eventual
 685 Gondwana breakup was likely driven by plate-scale tectonic processes (e.g. Merle, 2011; Murphy
 686 and Nance, 2013), with mantle convection or mantle plume processes being possible drivers (e.g.
 687 Weaver et al., 1994; Storey et al., 1999; Laird and Bradshaw, 2004). These processes are
 688 sufficiently large scale that they could have affected much of the Zealandia continental crust and
 689 may help explain the large size of the region of Zealandia that was impacted by normal faulting.

690

691 7. Conclusion

692 The Canterbury Basin in eastern Gondwana was deformed by normal faults from ~105 to
 693 ~85 Ma with general trends of NE-SW, E-W and NW-SE. These fault sets occur throughout the
 694 basin, although E-W and NE-SW trending structures dominate along the Chatham Rise and in the
 695 southern Canterbury Basin, respectively. Each of these fault sets is characterised by segmentation
 696 and relay ramps consistent with normal faulting. The predominance of normal faulting is further
 697 supported by horizontal separation diagrams and displacement analysis which indicate that all fault
 698 sets primarily accrued normal dip-slip, with displacement lows at segment boundaries; there is
 699 presently no evidence that segment boundaries have the pop-up or pull-apart basin geometries
 700 expected for strike-slip faults. Analysis of growth strata indicates that the three fault sets accrued
 701 displacements synchronously.

702 Our work supports the view that the Canterbury Basin accommodated multiple directions of
 703 extension coevally during the Late Cretaceous. The three fault sets are approximately parallel to
 704 spreading centres that define the present-day margins of Zealandia. NE-SW trending faults in the

705 southern basin were parallel to the mid-ocean ridge separating Southern Zealandia and western
 706 Antarctica, >500 km away from the Canterbury Basin. E-W and NW-SE rift faults were sub-
 707 parallel respectively to the spreading centre east of the Chatham Rise and the one between Australia
 708 and Northern Zealandia, both located >1000 km away from the Canterbury Basin. Basement
 709 structural fabric may have facilitated far field expression of these extension directions in the
 710 Canterbury Basin. These three sets of faults are also recognised across contemporaneous Late
 711 Cretaceous rift basins in Zealandia. The parallelism between spreading centres and normal faults
 712 suggests that multi-directional extension dominated the early stages of Gondwana breakup. The
 713 plate tectonic forces responsible for Gondwana breakup produced distributed stretching across
 714 much of Zealandia and influenced its continental crust for about 20 Myr prior to the onset of
 715 seafloor spreading. We argue that the Canterbury Basin multi-directional stretching differs from
 716 triple junction examples in that it was surrounded by multiple future spreading centres which varied
 717 in trend, stretching a large area of crust >4000 km by >1000 km. In the Canterbury Basin case, the
 718 initial phase of Gondwana breakup appears to have been characterised by mild (<20%) extension
 719 due to the large distance (>500 km) from future spreading centres along the Zealandia continental
 720 margin. With the onset of seafloor spreading at ~85 Ma, extension was focused along the spreading
 721 centres, and distributed stretching of Zealandia ceased or continued at much diminished rates.

722

723 Acknowledgement

724 We would like to thank A. Auzemery, S. Blanke, J. Bradshaw, F. Chanier, N. Mortimer and
 725 T. Sahoo for the discussions that helped several aspects of this paper, which promoted new ideas
 726 about Cretaceous faulting in the Canterbury Basin. GHB acknowledges funding from the NZ
 727 Government (MBIE) through Strategic Funding to GNS Science and the Sedimentary Basin
 728 Research programme. Finally, we would like to thank Mike Hall, Chris Morley, Cédric Bulois and

729 Tiago Alves for their journal reviews of the manuscript which helped improve its clarity and
 730 quality.

731

732 References

- 733 Adams, C. J., and J. I. Raine (1988), Age of Cretaceous silicic volcanism at Kyeburn, central Otago,
 734 and Palmerston, eastern Otago, South Island, New Zealand, *New Zealand Journal of Geology and*
 735 *Geophysics*, 31(4), 471-475.
- 736 Adams, C. J., H. J. Campbell, N. Mortimer, and W. L. Griffin (2017), Perspectives on Cretaceous
 737 Gondwana break-up from detrital zircon provenance of southern Zealandia sandstones, *Geological*
 738 *Magazine*, 154(4), 661-682.
- 739 Alves, T. M., and T. A. Cunha (2018), A phase of transient subsidence, sediment bypass and
 740 deposition of regressive-transgressive cycles during the breakup of Iberia and Newfoundland, *Earth*
 741 *and Planetary Science Letters*, 484, 168-183.
- 742 Arnot, M., K. Bland, A. Boyes, S. Bull, R. Funnell, A. Griffin, M. Hill, K. Kroeger, B. Lukovic,
 743 and P. Scadden (2016), Atlas of Petroleum Prospectivity, Northwest Province: ArcGIS geodatabase
 744 and technical report, *GNS Science Data Series 23b, 1*.
- 745 Bache, F., N. Mortimer, R. Sutherland, J. Collot, P. Rouillard, V. Stagpoole, and A. Nicol (2014),
 746 Seismic stratigraphic record of transition from Mesozoic subduction to continental breakup in the
 747 Zealandia sector of eastern Gondwana, *Gondwana Research*, 26(3), 1060-1078.
- 748 Barnes, P. M., F. C. Ghisetti, and A. R. Gorman (2016), New insights into the tectonic inversion of
 749 North Canterbury and the regional structural context of the 2010–2011 Canterbury earthquake
 750 sequence, New Zealand, *Geochemistry, Geophysics, Geosystems*, 17(2), 324-345.
- 751 Barrier, A. (2019), Tectonics, sedimentation and magmatism of the Canterbury Basin, New
 752 Zealand, *Unpublished PhD thesis, Christchurch. University of Canterbury*, 232.

- 753 Barrier, A., A. Nicol, G. H. Browne, and K. Bassett (2019), Early Oligocene marine canyon-
 754 channel systems: Implications for regional paleogeography in the Canterbury Basin, New Zealand,
 755 *Marine Geology*, 418, 106037, 16.
- 756 Bishop, D. G. (1974), Stratigraphic, structural, and metamorphic relationships in the Dansey Pass
 757 area, Otago, New Zealand, *New Zealand Journal of Geology and Geophysics*, 17(2), 301-335.
- 758 Bishop, D. G., M. G. Laird, and D. C. Mildenhall (1976), Stratigraphy and depositional
 759 environment of the kyeburn formation (cretaceous), a wedge of coarse terrestrial sediments in
 760 central otago, *Journal of the Royal Society of New Zealand*, 6(1), 55-71.
- 761 Bland, K. J., C. I. Uruski, and M. J. Isaac (2015), Pegasus Basin, eastern New Zealand: A
 762 stratigraphic record of subsidence and subduction, ancient and modern, *New Zealand Journal of
 763 Geology and Geophysics*, 58(4), 319-343.
- 764 Browne, G. H., B. D. Field, D. J. A. Barrell, R. Jongens, K. N. Bassett, and R. A. Wood (2012), The
 765 geological setting of the Darfield and Christchurch earthquakes, *New Zealand Journal of Geology
 766 and Geophysics*, 55(3), 193-197.
- 767 Browne GH, Sahoo TR, Campbell HJ. 2013. The Tupuangi Formation, Pitt Island: seismic and
 768 reservoir characteristics of a mid-Cretaceous deltaic succession exposed in the Chatham Islands.
- 769 Brune, S., S. E. Williams, N. P. Butterworth, and R. D. Müller (2016), Abrupt plate accelerations
 770 shape rifted continental margins, *Nature*, 536(7615), 201.
- 771 Carter, L., and R. M. Carter (1993), Sedimentary evolution of the Bounty Trough: a Cretaceous rift
 772 basin, southwestern Pacific Ocean, *South Pacific Sedimentary Basins. Sedimentary Basins of the
 773 World*, 2, 51-67.
- 774 Carter, R., L. Carter, and B. Davy (1994), Seismic stratigraphy of the Bounty Trough, south-west
 775 Pacific Ocean, *Marine and Petroleum Geology*, 11(1), 79-93.
- 776 Childs, C., J. Watterson, and J. Walsh (1995), Fault overlap zones within developing normal fault
 777 systems, *Journal of the Geological Society*, 152(3), 535-549.

- 778 Childs, C., R. E. Holdsworth, C. A.-L. Jackson, T. Manzocchi, J. J. Walsh, and G. Yielding (2017),
 779 Introduction to the geometry and growth of normal faults, *Geological Society, London, Special*
 780 *Publications*, 439, 10.
- 781 Cooper, R. A. E. (2004), The New Zealand Geological Timescale, 22, 284.
- 782 Coward, M., J. Dewey, M. Hempton, and J. Holroyd (2003), Tectonic evolution, *The Millennium*
 783 *Atlas: Petroleum Geology of the Central and Northern North Sea. Geological Society, London*, 17,
 784 33.
- 785 Crampton, J. S., N. Mortimer, K. J. Bland, D. P. Strogen, M. Sagar, B. R. Hines, P. R. King, and H.
 786 Seebeck (2019), Cretaceous termination of subduction at the Zealandia margin of Gondwana: The
 787 view from the paleo-trench, *Gondwana Research*, 70, 222-242.
- 788 Davison, I., and J. R. Underhill (2012), Tectonics and Sedimentation in Extensional Rifts:
 789 Implications for Petroleum Systems, in *Tectonics and sedimentation: Implications for petroleum*
 790 *systems*, edited by D. Gao, pp. 15-42, American Association of Petroleum Geologists.
- 791 Davy, B. (2014), Rotation and offset of the Gondwana convergent margin in the New Zealand
 792 region following Cretaceous jamming of Hikurangi Plateau large igneous province subduction,
 793 *Tectonics*, 33(7-8), 1577-1595.
- 794 Deckert, H., U. Ring, and N. Mortimer (2002), Tectonic significance of Cretaceous bivergent
 795 extensional shear zones in the Torlesse accretionary wedge, central Otago Schist, New Zealand,
 796 *New Zealand Journal of Geology and Geophysics*, 45(4), 537-547.
- 797 Dunbar, J. A., and D. S. Sawyer (1996), Three-dimensional dynamical model of continental rift
 798 propagation and margin plateau formation, *Journal of Geophysical Research: Solid Earth*,
 799 101(B12), 27845-27863.
- 800 Field, B. D., and G. H. Browne (1989), Cretaceous and cenozoic sedimentary basins and geological
 801 evolution of the Canterbury Region, South Island, New Zealand, *Institute of Geological & Nuclear*
 802 *Sciences Monograph*, 2, 94.

- 803 Grindley, G., and F. Davey (1982), The reconstruction of New Zealand, Australia and Antarctica,
 804 *Antarctic geoscience*, 15-29.
- 805 Heine, C., J. Zoethout, and R. D. Müller (2013), Kinematics of the South Atlantic rift, *Solid Earth*,
 806 4, 215-253.
- 807 Henza, A. A., M. O. Withjack, and R. W. Schlische (2010), Normal-fault development during two
 808 phases of non-coaxial extension: An experimental study, *Journal of Structural Geology*, 32(11),
 809 1656-1667.
- 810 Higgs, K. E., G. H. Browne, and T. R. Sahoo (2019), Reservoir characterisation of syn-rift and post-
 811 rift sandstones in frontier basins: An example from the Cretaceous of Canterbury and Great South
 812 basins, New Zealand, *Marine and Petroleum Geology*, 101, 1-29.
- 813 Huismans, R., and C. Beaumont (2011), Depth-dependent extension, two-stage breakup and
 814 cratonic underplating at rifted margins, *Nature*, 473(7345), 74-78.
- 815 Jongens, R., D. J. A. Barrell, J. K. Campbell, and J. R. Pettinga (2012), Faulting and folding
 816 beneath the Canterbury Plains identified prior to the 2010 emergence of the Greendale Fault, *New
 817 Zealand Journal of Geology and Geophysics*, 55(3), 169-176.
- 818 King, P. R. (2000), Tectonic reconstructions of New Zealand: 40 Ma to the Present, *New Zealand
 819 Journal of Geology and Geophysics*, 43(4), 611-638.
- 820 King, P. R., T. R. Naish, G. H. Browne, B. D. Field, and S. W. Edbrooke (1999), Cretaceous to
 821 Recent sedimentary patterns in New Zealand, *Institute of Geological and Nuclear Sciences Folio
 822 Series 1*, 35.
- 823 Koptev, A., T. Gerya, E. Calais, S. Leroy, and E. Burov (2018), Afar triple junction triggered by
 824 plume-assisted bi-directional continental break-up, *Scientific reports*, 8(14742), 7.
- 825 Laird, M. G. (1993), Cretaceous continental rifts: New Zealand region, in *Sedimentary basins of the
 826 world* , edited by P. E. Ballance, pp. 37-49, Elsevier Science Publisher.
- 827 Laird, M. G., and J. D. Bradshaw (2004), The Break-up of a Long-term Relationship: the
 828 Cretaceous Separation of New Zealand from Gondwana, *Gondwana Research*, 7(1), 273-286.

- 829 Lamb, S., N. Mortimer, E. Smith, and G. Turner (2016), Focusing of relative plate motion at a
 830 continental transform fault: Cenozoic dextral displacement > 700 km on New Zealand's Alpine
 831 Fault, reversing > 225 km of Late Cretaceous sinistral motion, *Geochemistry, Geophysics,
 832 Geosystems*, 17(3), 1197-1213.
- 833 Lei, C., T. M. Alves, J. Ren, X. Pang, L. Yang, and J. Liu (2019), Depositional architecture and
 834 structural evolution of a region immediately inboard of the locus of continental breakup (Liwan
 835 Sub-basin, South China Sea), *Bulletin*, 131(7-8), 1059-1074.
- 836 Massironi, M., G. Di Achille, D. A. Rothery, V. Galluzzi, L. Giacomini, S. Ferrari, M. Zusi, G.
 837 Cremonese, and P. Palumbo (2015), Lateral ramps and strike-slip kinematics on Mercury,
 838 *Geological Society, London, Special Publications*, 401(1), 269-290.
- 839 McFadden, R., C. Teyssier, C. S. Siddoway, M. A. Cosca, and C. M. Fanning (2015), Mid-
 840 Cretaceous oblique rifting of West Antarctica: Emplacement and rapid cooling of the Fosdick
 841 Mountains migmatite-cored gneiss dome, *Lithos*, 232, 306-318.
- 842 Merle, O. (2011), A simple continental rift classification, *Tectonophysics*, 513(1-4), 88-95.
- 843 Meyer, V., A. Nicol, C. Childs, J. Walsh, and J. Watterson (2002), Progressive localisation of strain
 844 during the evolution of a normal fault population, *Journal of Structural Geology*, 24(8), 1215-1231.
- 845 Mitchell, M., D. Craw, C. A. Landis, and R. Frew (2009), Stratigraphy, provenance, and diagenesis
 846 of the Cretaceous Horse Range Formation, east Otago, New Zealand, *New Zealand Journal of
 847 Geology and Geophysics*, 52(3), 171-183.
- 848 Mohr, P. (1970), The Afar Triple Junction and sea-floor spreading, *Journal of Geophysical
 849 Research*, 75(35), 7340-7352.
- 850 Morley, C., C. Haranya, W. Phoosongsee, S. Pongwapee, A. Kornsawan, and N. Wonganan (2004),
 851 Activation of rift oblique and rift parallel pre-existing fabrics during extension and their effect on
 852 deformation style: examples from the rifts of Thailand, *Journal of Structural Geology*, 26(10),
 853 1803-1829. Morley, C. K. (2017), The impact of multiple extension events, stress rotation and

- 854 inherited fabrics on normal fault geometries and evolution in the Cenozoic rift basins of Thailand,
 855 *Geological Society, London, Special Publications*, 439(1), 413-445.
- 856 Mortimer, N. (1993), Geology of the Otago schist and adjacent rocks. Scale 1:500 000., *Lower*
 857 *Hutt: Institute of Geological & Nuclear Sciences.*, *Institute of Geological & Nuclear Sciences*
 858 *geological map 7.*
- 859 Mortimer, N. (2000), Metamorphic discontinuities in orogenic belts: example of the garnet–biotite–
 860 albite zone in the Otago Schist, New Zealand, *International Journal of Earth Sciences*, 89(2), 295–
 861 306.
- 862 Mortimer, N. (2004), New Zealand's geological foundations, *Gondwana Research*, 7(1), 261-272.
- 863 Mortimer, N. (2018), Evidence for a pre-Eocene proto-Alpine Fault through Zealandia, *New*
 864 *Zealand Journal of Geology and Geophysics*, 61(3), 1-9.
- 865 Mortimer, N., A. J. Tulloch, R. N. Spark, N. W. Walker, E. Ladley, A. Allibone, and D. L.
 866 Kimbrough (1999), Overview of the Median Batholith, New Zealand: a new interpretation of the
 867 geology of the Median Tectonic Zone and adjacent rocks, *Journal of African Earth Sciences*, 29(1),
 868 257-268.
- 869 Mortimer, N., P. van den Bogaard, K. Hoernle, C. Timm, P. Gans, R. Werner, and F. Riefstahl
 870 (2019), Late Cretaceous oceanic plate reorganization and the breakup of Zealandia and Gondwana,
 871 *Gondwana Research*, 65, 31-42.
- 872 Mortimer, N., H.J. Campbell, A.J. Tulloch, P.R. King, V.M. Stagpoole, R.A. Wood, M.S.
 873 Rattenbury, R. Sutherland, C.J. Adams, J. Collot, M. Seton (2017), Zealandia: Earth's hidden
 874 Continent, *GSA Today*, 27(3-4), 27-35.
- 875 Mortimer, N., M.S. Rattenbury, P.R. King, K.J. Bland, D.J.A. Barrell, F. Bache, J.G. Begg, H.J.
 876 Campbell, S.C. Cox, J.S. Crampton, S.W. Edbrooke, P.J. Forsyth, M.R. Johnston, R. Jongens, J.M.
 877 Lee, G.S. Leonard, J.I. Raine, D.N.B. Skinner, C. Timm, D.B. Townsend, A.J. Tulloch, I.M.
 878 Turnbull , R.E. Turnbull (2014), High-level stratigraphic scheme for New Zealand rocks, *New*
 879 *Zealand Journal of Geology and Geophysics*, 57(4), 402-419.

- 880 Müller, R. D., C. Gaina, and S. Clark (2000), Seafloor spreading around Australia, *Billion-year*
 881 *earth history of Australia and neighbours in Gondwanaland*, 18-28.
- 882 Murphy, J. B., and R. D. Nance (2013), Speculations on the mechanisms for the formation and
 883 breakup of supercontinents, *Geoscience Frontiers*, 4(2), 185-194.
- 884 Nicol, A., J. Walsh, C. Childs, and T. Manzocchi (2020), The growth of faults, in *Understanding*
 885 *Faults*, edited, pp. 221-255, Elsevier.
- 886 Philippon, M., E. Willingshofer, D. Sokoutis, G. Corti, F. Sani, M. Bonini, and S. Cloetingh (2015),
 887 Slip re-orientation in oblique rifts, *Geology*, 43(2), 147-150.
- 888 Phillips, T. B., and K. J. McCaffrey (2019), Terrane boundary reactivation, barriers to lateral fault
 889 propagation and reactivated fabrics□Rifting across the Median Batholith Zone, Great South Basin,
 890 New Zealand, *Tectonics*.
- 891 Raine, J. I., A. G. Beu, A. F. Boyes, H. J. Campbell, R. A. Cooper, J. S. Crampton, M. P.
 892 Crundwell, C. J. Hollis, H. E. G. Morgans, and N. Mortimer (2015), New Zealand Geological
 893 Timescale NZGT 2015, *New Zealand Journal of Geology and Geophysics*, 58(4), 398-403.
- 894 Ravnås, R., and R. J. Steel (1998), Architecture of marine rift-basin successions, *AAPG Bulletin*,
 895 82(1), 110-146.
- 896 Rieftahl, F., K. Gohl, B. Davy, K. Hoernle, N. Mortimer, C. Timm, R. Werner, and K. Hochmuth
 897 (2019), Cretaceous intracontinental rifting at the southern Chatham Rise margin and initialisation of
 898 seafloor spreading between Zealandia and Antarctica, *Tectonophysics*, 228-298.
- 899 Ring, U., C. Betzler, and D. Delvaux (1992), Normal vs. strike-slip faulting during rift development
 900 in East Africa: the Malawi rift, *Geology*, 20(11), 1015-1018.
- 901 Sahoo, T., K. Bland, M. Arnot, A. Boyes, R. Funnell, A. Griffin, K. Kroeger, M. Lawrence, G.
 902 O'Brien, and P. Scadden (2017), Atlas of Petroleum Prospectivity, Southeast Province: ArcGIS
 903 geodatabase and technical report, *GNS Science Data Series 23c, 1*.

- 904 Sahoo, T. R., P. R. King, K. J. Bland, D. P. Strogen, R. Sykes, and F. Bache (2014), Tectono-
 905 sedimentary evolution and source rock distribution of the mid to Late Cretaceous succession in
 906 Great South Basin, New Zealand, *APPEA Journal*, 54(July 2016), 259-274.
- 907 Sahoo, T. R., K. F. Kroeger, G. Thrasher, S. Munday, H. Mingard, N. Cozens, and M. Hill (2015),
 908 Facies Distribution and Impact on Petroleum Migration in the Canterbury Basin , New Zealand, *In:*
 909 *Eastern Australian Basins Symposium 2015: Publication of Proceedings. Petroleum Exploration*
 910 *Society of Australia, Perth, WA*, 187-202.
- 911 Salerno, V. M., F. A. Capitanio, R. J. Farrington, and N. Riel (2016), The role of long-term rifting
 912 history on modes of continental lithosphere extension, *Journal of Geophysical Research: Solid*
 913 *Earth*, 121(12), 8917-8940.
- 914 Schiøler, P., and J. I. Raine, compilers (2011), Revised Biostratigraphy and Well Correlation,
 915 Canterbury Basin, New Zealand, *Ministry of Economic Development New Zealand Unpublished*
 916 *Petroleum Report PR4365*, 142.
- 917 Soares, D. M., T. M. Alves, and P. Terrinha (2012), The breakup sequence and associated
 918 lithospheric breakup surface: Their significance in the context of rifted continental margins (West
 919 Iberia and Newfoundland margins, North Atlantic), *Earth and Planetary Science Letters*, 355, 311-
 920 326.
- 921 Soares, D. M., T. M. Alves, and P. Terrinha (2014), Contourite drifts on early passive margins as an
 922 indicator of established lithospheric breakup, *Earth and Planetary Science Letters*, 401, 116-131.
- 923 Stagpoole, V., and A. Nicol (2008), Regional structure and kinematic history of a large subduction
 924 back thrust: Taranaki Fault, New Zealand, *Journal of Geophysical Research: Solid Earth*, 113(B1),
 925 19.
- 926 Storey, B. C. (1995), The role of mantle plumes in continental breakup: case histories from
 927 Gondwanaland, *Nature*, 377(6547), 301-308.

- 928 Storey, B. C., P. T. Leat, S. D. Weaver, R. J. Pankhurst, J. D. Bradshaw, and S. Kelley (1999),
 929 Mantle plumes and Antarctica-New Zealand rifting: evidence from mid-Cretaceous mafic dykes,
 930 *Journal of the Geological Society*, 156(4), 659-671.
- 931 Strogen, D., P., and P. R. King (2014), A new Zealandia-wide seismic horizon naming scheme,
 932 *GNS Science Report*, 2014/34, 20.
- 933 Strogen, D. P., H. Seebeck, A. Nicol, and P. R. King (2017), Two-phase Cretaceous – Paleocene
 934 rifting in the Taranaki Basin region, New Zealand; implications for Gondwana break-up, *Journal of*
 935 *the Geological Society*, 174, 929-946.
- 936 Strogen, D. P., K. E. Higgs, A. G. Griffin, and H. E. G. Morgans (2019), Late Eocene – Early
 937 Miocene facies and stratigraphic development, Taranaki Basin, New Zealand: the transition to plate
 938 boundary tectonics during regional transgression, *Geological Magazine*, 1-20.
- 939 Sutherland, R. (1999), Basement geology and tectonic development of the greater New Zealand
 940 region: an interpretation from regional magnetic data, *Tectonophysics*, 308(3), 341-362.
- 941 Taylor, S. K., A. Nicol, and J. J. Walsh (2008), Displacement loss on growth faults due to sediment
 942 compaction, *Journal of Structural Geology*, 30(3), 394-405.
- 943 Tulloch, A., et al. (2019), Reconnaissance basement geology and tectonics of South Zealandia,
 944 *Tectonics*, 38(2), 516-551.
- 945 Tulloch, A. J., J. Ramezani, N. Mortimer, J. Mortensen, P. van den Bogaard, and R. Maas (2009),
 946 Cretaceous felsic volcanism in New Zealand and Lord Howe Rise (Zealandia) as a precursor to
 947 final Gondwana break-up, *Geological Society, London, Special Publications*, 321(1), 89-118.
- 948 Ulvrova, M. M., S. Brune, and S. Williams (2019), Breakup without borders: how continents speed
 949 up and slow down during rifting, *Geophysical Research Letters*, 46(3), 1338-1347.
- 950 Walsh, J., C. Childs, V. Meyer, T. Manzocchi, J. Imber, A. Nicol, G. Tuckwell, W. Bailey, C.
 951 Bonson, and J. Watterson (2001), Geometric controls on the evolution of normal fault systems,
 952 *Geological Society, London, Special Publications*, 186(1), 157-170.

- 953 Walsh, J. J., J. Watterson, W. R. Bailey, and C. Childs (1999), Fault relays, bends and branch-lines,
 954 *Journal of Structural Geology*, 21(8), 1019-1026.
- 955 Watterson, J., J. Walsh, P. Gillespie, and S. Easton (1996), Scaling systematics of fault sizes on a
 956 large-scale range fault map, *Journal of Structural Geology*, 18(2-3), 199-214.
- 957 Weaver, S., B. Storey, R. Pankhurst, S. Mukasa, V. DiVenere, and J. Bradshaw (1994), Antarctica-
 958 New Zealand rifting and Marie Byrd Land lithospheric magmatism linked to ridge subduction and
 959 mantle plume activity, *Geology*, 22(9), 811-814.
- 960 Wood, R., and H. Anderson (1989), Basement structure at the Chatham Islands, *Journal of the
 961 Royal Society of New Zealand*, 19(3), 269-282.
- 962 Wood, R. A., and R. H. Herzer (1993), The Chatham Rise, New Zealand, in *South Pacific
 963 Sedimentary Basins*, edited by P. F. Ballance, pp. 329-349, Elsevier Science Publishers,
 964 Amsterdam.
- 965 Wood, R. A., Andrews, P. B., Herzer, R. H., & Cook, R. A. (1989), Cretaceous and Cenozoic
 966 geology of the Chatham Rise region, South Island, New Zealand, *New Zealand Geological Survey
 967 Basin Studies 3*, 75.
- 968 Wright, N. M., M. Seton, S. E. Williams, and R. D. Mueller (2016), The Late Cretaceous to recent
 969 tectonic history of the Pacific Ocean basin, *Earth-Science Reviews*, 154, 138-173.
- 970 Zampieri, D., M. Massironi, R. Seda, and V. Sparacino (2003), Strike-slip contractional stepovers
 971 in the Southern Alps (northeastern Italy), *Eclogae Geologicae Helvetiae*, 96(1), 115-124.
- 972 Zanella, E., M. Coward, D. Evans, C. Graham, A. Armour, and P. Bathurst (2003), Structural
 973 framework, *The Millennium Atlas: Petroleum Geology of the Central and Northern North Sea.
 974 Geological Society, London*, 45, 59.
- 975 Zhao, F., T. M. Alves, S. Wu, W. Li, M. Huuse, L. Mi, Q. Sun, and B. Ma (2016), Prolonged post-
 976 rift magmatism on highly extended crust of divergent continental margins (Baiyun Sag, South
 977 China Sea), *Earth and Planetary Science Letters*, 445, 79-91.

Journal Pre-proof

979 Supplementary Material 1 : Un-interpreted seismic profiles of Figure 12.

980 **SUPPLEMENTARY MATERIAL 1 HERE (FILE SOURCE>10 MB)**

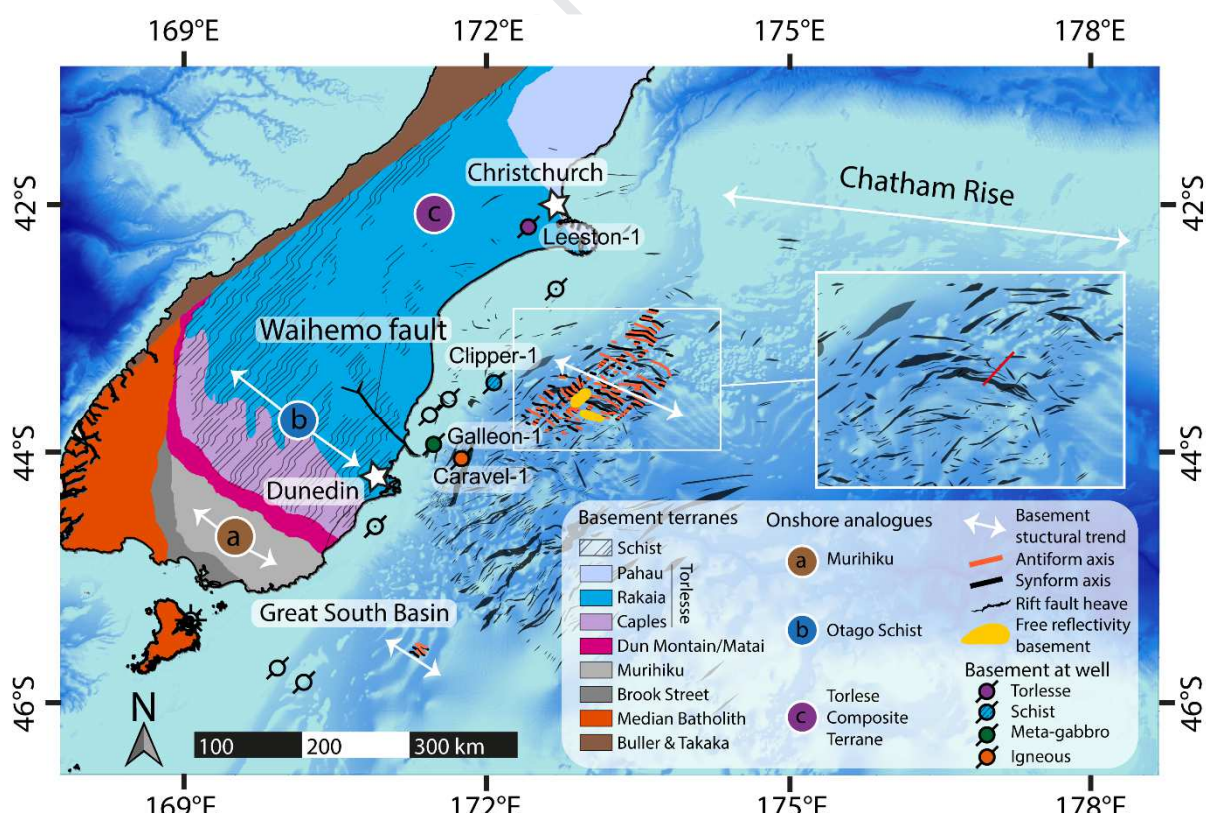
981

982 Supplementary Material 2 : Seismic reflection profile offshore Canterbury Basin showing basement
983 reflectivity and rift faults. Green reflector package corresponds to syn-rift sequence. Yellow
984 reflector package corresponds to post-rift sequence.

985 **SUPPLEMENTARY MATERIAL 2 HERE (FILE SOURCE>10 MB)**

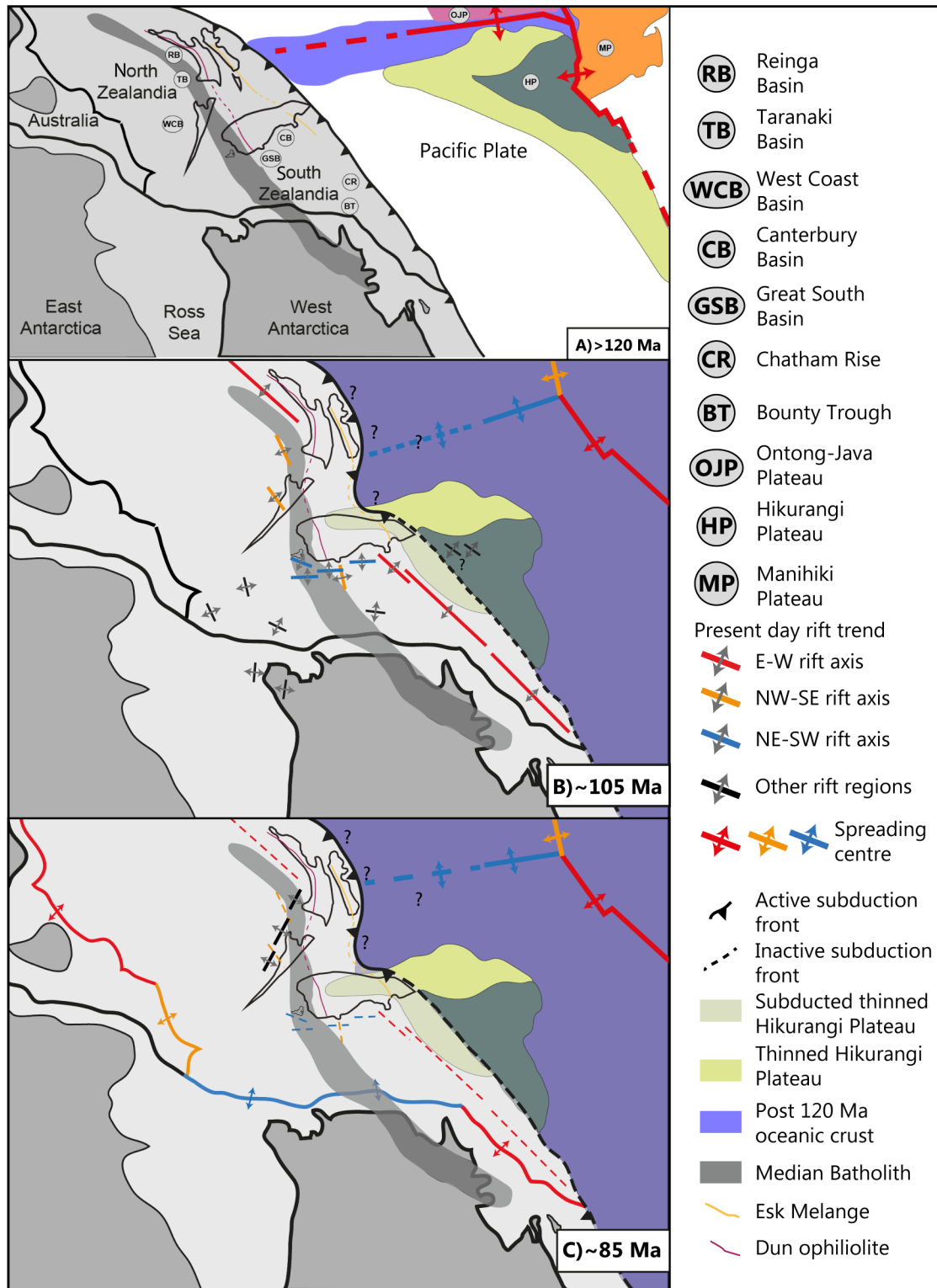
986

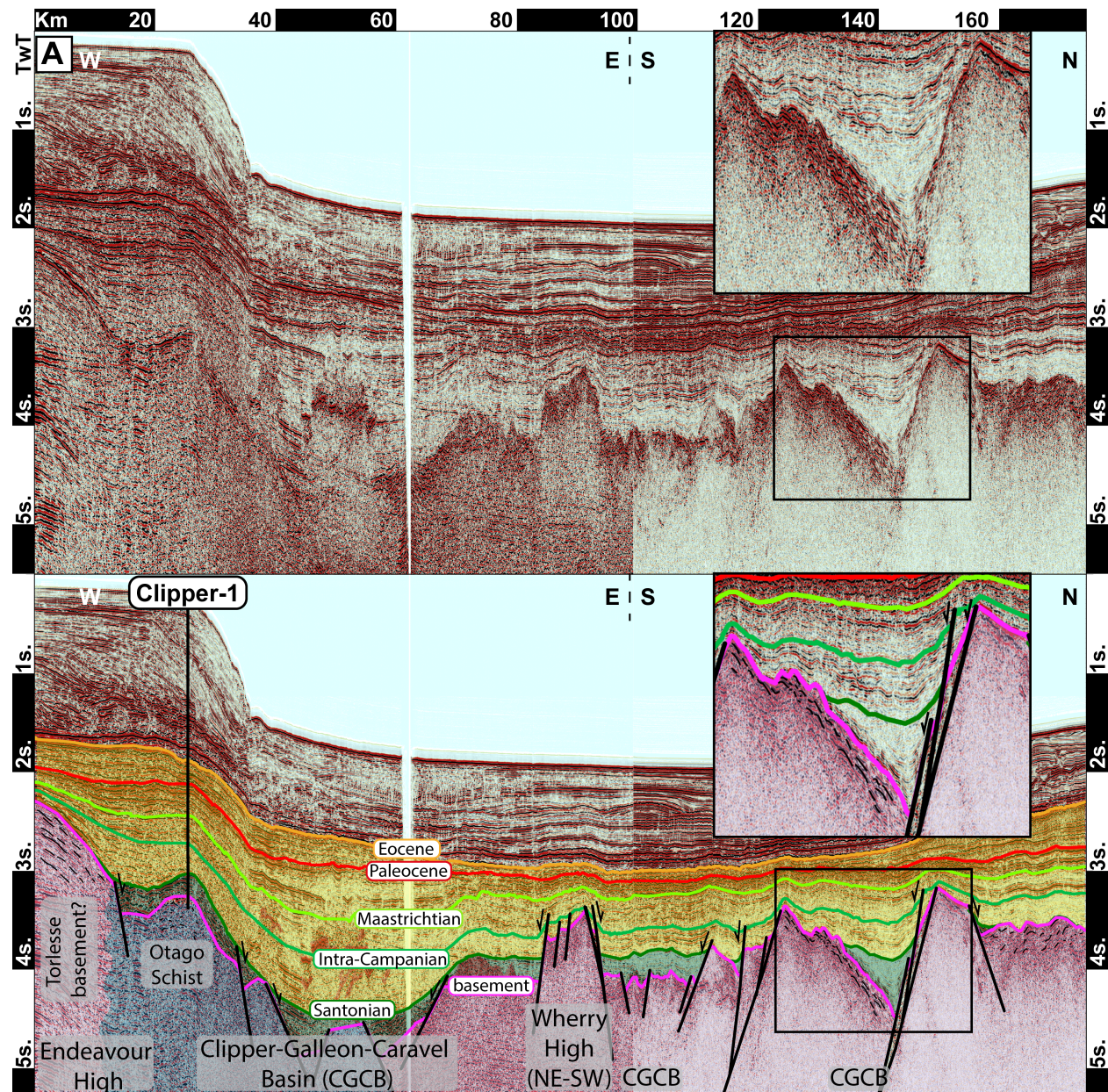
987 Supplementary Material 3 : Map showing the fold axis mapped in the Canterbury and Great South
988 Basin, the basement lithology at the bottom of exploration wells and the onshore basement terranes.
989 Red line represents the location of supplementary Material 4

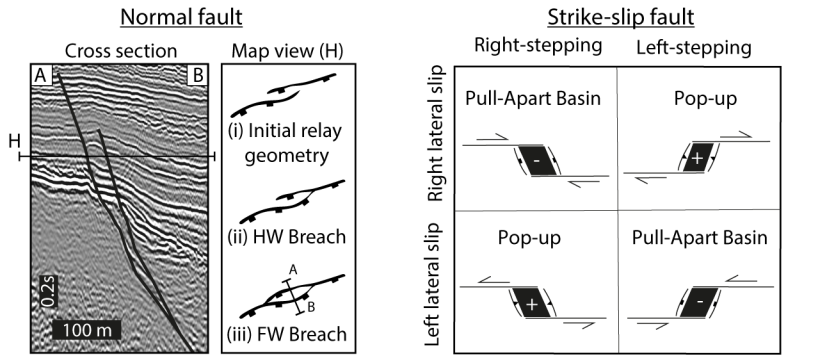
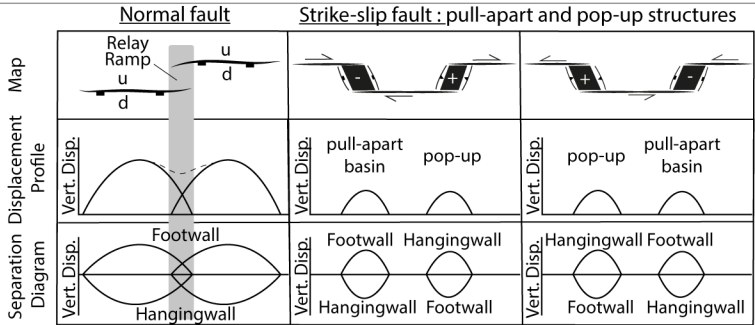
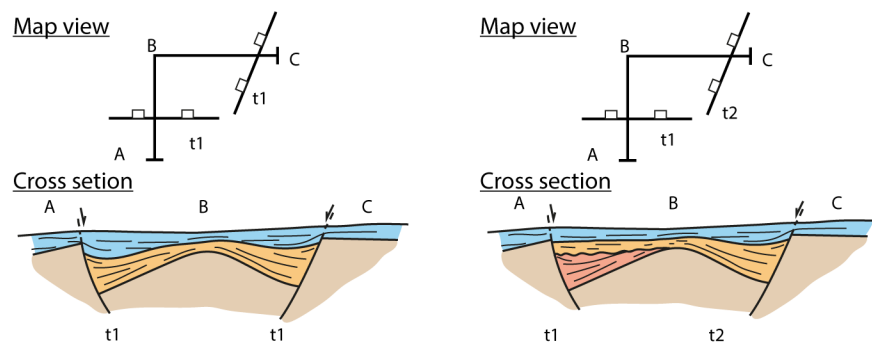


990

991





A/ Architecture at fault tips**B/ Fault kinematics****C/ Rift fault synchronicity**

Highlights (3-5; 85 characters/bullet point)

- The Canterbury Basin rift (~105-85 Ma) produced NE-SW, E-W and NW-SE rift faults.
- These sets of faults are coeval and have normal fault geometries and displacements.
- The three fault sets are parallel to spreading centres of similar orientations.
- Multiple directions of extension produced mild (<20%) distributed stretching.
- Results show an onset of fragmentation of eastern Gondwana ~20 Myr before breakup.